Measurement of the F_2^n/F_2^p, d/u **RA**tios and A=3 EMC Effect in Deep Inelastic Electron Scattering off the **T**ritium and **H**elium Mirr**O**r **N**uclei.

Jefferson Lab PAC30 Proposal, July 2006

The JLab **MARATHON** Collaboration

J. Arrington, D. F. Geesaman, K. Hafidi, R. Holt, D. Potterveld,
P. Reimer, P. Solvignon
Argonne National Laboratory, Argonne, Illinois, USA

K. A. Aniol, D. J. Margaziotis, M. B. Epstein
California State University, Los Angeles, California, USA

G. Fanourakis
Demokritos National Center for Scientific Research, Athens, Greece

J. Annand, D. Ireland, R. Kaiser, G. Rosner
University of Glasgow, Scotland, UK

E. Cisbani, F. Cussano, S. Frullani, F. Garibaldi, M. Iodice, L. Lagamba,
R. De Leo, E. Pace, G. Salmè, G. M. Urciuoli
Istituto Nazionale di Fisica Nucleare, Rome and Bari, Italy

E. Chudakov, J. Gomez, J.-O. Hansen, D. Higinbotham, C. W. de Jager, J. LeRose,
W. Melnitchouk, R. Michaels, S. K. Nanda, A. Saha, B. Wojtsekhowski
Jefferson Lab, Newport News, Virginia, USA

B. D. Anderson, A. T. Katramatou, E. Khrosinkova, D. M. Manley,
S. Margetis, G. G. Petratos, W.-M. Zhang
Kent State University, Kent, Ohio, USA

J. R. Calarco
University of New Hampshire, Durham, New Hampshire, USA

C. Ciofi degli Atti, S. Scopetta
University of Perugia, Perugia, Italy

R. Gilman, C. Glashausser, R. D. Ransome, X. Jiang
Rutgers, The State University of New Jersey, New Brunswick, New Jersey, USA

M. N. Olson
St. Norbert College, De Pere, Wisconsin, USA

S. Liuti, O. Rondon
University of Virginia, Charlottesville, Virginia, USA

Spokesperson: G. G. Petratos (gpetrato@kent.edu)

Co-spokespersons: J. Gomez, R. Holt and R. D. Ransome

ABSTRACT

We propose to perform deep inelastic electron scattering of the ^{3}H and ^{3}He mirror nuclei with the 11 GeV upgraded beam of Jefferson Lab. The experiment will measure the EMC effect ratio for ^{3}H and ^{3}He and will determine the ratio of the neutron to proton inelastic structure functions, F_2^n/F_2^p, and the ratio of the down to up quark distributions in the nucleon, d/u, at medium and large Bjorken x. It will use a cryogenic ^{3}H and ^{3}He gas target system operating at 45 K and 15 atm, and the Hall A High Resolution Spectrometers. The required beam time is 31 days at a beam current of 70 μA. The F_2^n/F_2^p ratio will be extracted from the inelastic cross section ratio of the two nuclei by exploiting their mirror symmetry with a minimal theoretical correction. The F_2^n/F_2^p ratio is expected to be almost free of nuclear effects, which introduce a significant uncertainty in its extraction from deep inelastic scattering off the proton and deuteron. The results are expected to test perturbative and non-perturbative mechanisms of spin-flavor symmetry breaking in the nucleon, and constrain the structure function parametrizations needed for the interpretation of high energy hadron collider data. The precision of the expected data for the ratio of the EMC effect for ^{3}H and ^{3}He will offer a unique opportunity to test competing parametrizations and calculations of the EMC effect and will provide critical experimental input for the establishment of a unique canonical model for the explanation of its dynamical origin. The Collaboration intends to submit follow-up proposals for measurements of elastic and quasielastic scattering off ^{3}H at large momentum transfers. The latter measurements will complement similar existing or planned measurements off ^{3}He and will provide valuable data for our understanding of the structure and dynamics of the three-body nuclear systems.

1 Introduction

Measurements of the proton and deuteron structure functions have been of fundamental importance in establishing the internal quark structure of the nucleon [1, 2, 3]. The first evidence for the presence of point-like constituents (partons) in the nucleon came from the observation that the ratio of inelastic to Mott electron-proton cross sections, measured in the pioneering SLAC experiments, exhibited only small variation with momentum transfer [4]. The subsequent detailed analysis of the SLAC data [5] revealed the predicted "scaling pattern" [6] in the nucleon structure functions, consistent with scattering from partons carrying the quantum numbers of the Gell-Mann/Zweig quarks. Further experimental studies of muon-nucleon and neutrino-nucleon inelastic scattering experiments at CERN and Fermilab established beyond any doubt the quark-parton model (QPM) of the nucleon [7], and provided substantial supporting evidence for the emerging theory of quantum chromodynamics (QCD) [8].

The cross section for inelastic electron-nucleon scattering is given in terms of the structure functions $F_1(\nu, Q^2)$ and $F_2(\nu, Q^2)$ of the nucleon by:

$$\sigma \equiv \frac{d^2\sigma}{d\Omega dE'}(E, E', \theta) = \frac{4\alpha^2(E')^2}{Q^4}\cos^2(\frac{\theta}{2})\left[\frac{F_2(\nu, Q^2)}{\nu} + \frac{2F_1(\nu, Q^2)}{M}\tan^2(\frac{\theta}{2})\right] \ , \qquad (1)$$

where α is the fine-structure constant, E is the incident electron energy, E' and θ are the scattered electron energy and angle, $\nu = E - E'$ is the energy transfer, $Q^2 = 4EE'\sin^2(\theta/2)$ is minus the four-momentum transfer squared, and M is the nucleon mass.

The basic idea of the quark-parton model [6, 9] is to represent inelastic electron-nucleon scattering as quasi-free scattering from the partons/quarks in the nucleon, when viewed in a frame where the nucleon has infinite momentum (the center-of-mass frame is a very good approximation to such a frame). The fractional momentum of the nucleon carried by the struck quark is given by the Bjorken scaling variable, $x = Q^2/2M\nu$. In the limit where $\nu \to \infty$, $Q^2 \to \infty$ with x fixed, the nucleon structure functions become:

$$F_1 = \frac{1}{2}\sum_i e_i^2 q_i(x) \ , \qquad F_2 = x\sum_i e_i^2 q_i(x) \ . \qquad (2)$$

Here, e_i is the fractional charge of quark type i, $q_i(x)dx$ is the probability that a quark of

type i carries momentum in the range between x and $x+dx$, and the sum runs over all quark types.

Since the charges of the u, d and s quarks are $2/3$, $-1/3$ and $-1/3$, respectively, the $F_2(x)$ structure function for the proton is given by:

$$F_2^p(x) = x\left[\left(\frac{2}{3}\right)^2(u+\bar{u}) + \left(-\frac{1}{3}\right)^2\left(d+\bar{d}\right) + \left(-\frac{1}{3}\right)^2(s+\bar{s})\right]. \tag{3}$$

The parton distribution functions in the neutron are related to those in the proton by isospin symmetry. Since the up/down quarks and proton/neutron both form isospin doublets, one has: $u^p(x) = d^n(x) \equiv u(x)$, $d^p(x) = u^n(x) \equiv d(x)$, $s^p(x) = s^n(x) \equiv s(x)$ (with analogous relations for the antiquarks), and:

$$F_2^n(x) = x\left[\left(-\frac{1}{3}\right)^2(u+\bar{u}) + \left(\frac{2}{3}\right)^2\left(d+\bar{d}\right) + \left(-\frac{1}{3}\right)^2(s+\bar{s})\right]. \tag{4}$$

Equations 3 and 4 result in the structure function ratio:

$$\frac{F_2^n}{F_2^p} = \frac{[(u+\bar{u})+(s+\bar{s})]+4(d+\bar{d})}{4(u+\bar{u})+[(d+\bar{d})+(s+\bar{s})]}\ . \tag{5}$$

Since all the quark distribution functions must be positive for all x, the above expression is bounded for all x by:

$$\frac{1}{4} \leq \frac{F_2^n}{F_2^p} \leq 4\ , \tag{6}$$

which is known as the Nachtmann inequality [10]. If one neglects the strange quarks and antiquarks, Equation 5 yields the well known simple relationship:

$$\frac{F_2^n}{F_2^p} = \frac{[(u+\bar{u})]+4(d+\bar{d})}{4(u+\bar{u})+[(d+\bar{d})]} = \frac{1+4(D/U)}{4+(D/U)}\ , \tag{7}$$

where $U = u + \bar{u}$ and $D = d + \bar{d}$. For the remainder of this proposal the notation D/U will be replaced, as it is customary, simply by d/u, with d and u denoting quark plus antiquark distributions. Figure 1 shows all the SLAC data from the pioneering SLAC/MIT Collaboration experiments on the F_2^n/F_2^p ratio versus x [11]. The ratio has been extracted from deep inelastic scattering (DIS) (large Q^2 and ν) measurements off the proton and deuteron, using a smearing model to account for the Fermi-motion of the nucleons in the deuteron [12]. The ratio data are within the bounds of the Nachtmann inequality. For large x, the ratio is about $1/4$ which can only be reached if $d = \bar{d} = s = \bar{s} = 0$. This suggests a

picture in which the high momentum partons in the proton (neutron) are mainly up (down) quarks. For small x, the ratio is close to 1, suggesting little influence of valence quarks and dominance of the quark-antiquark "sea".

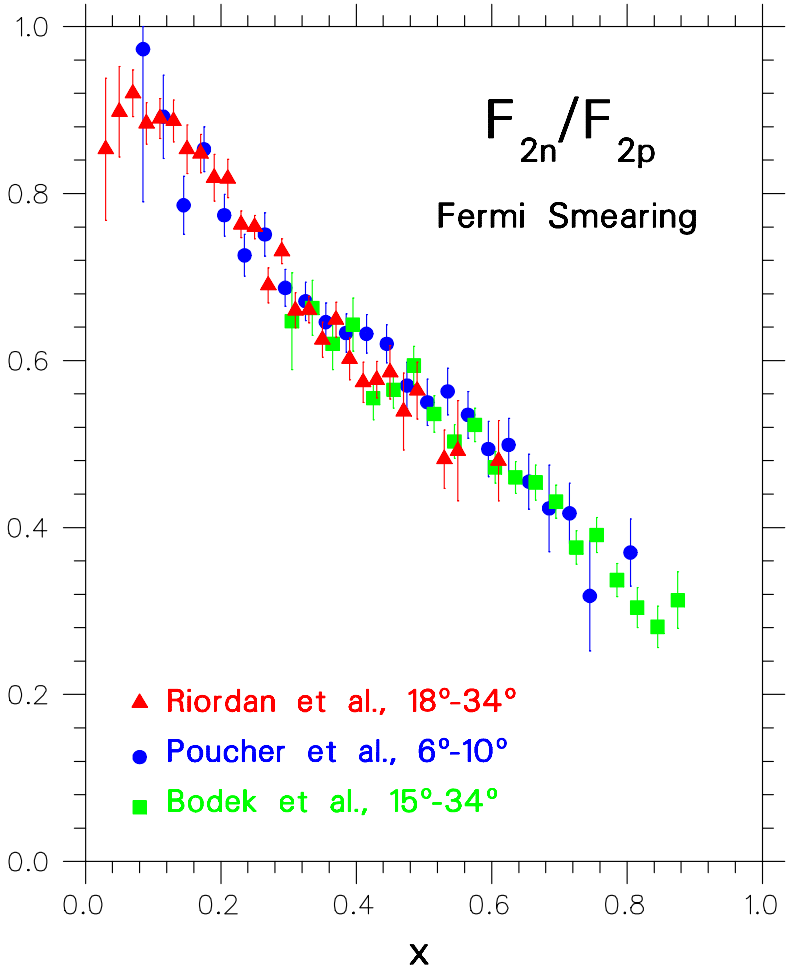

Figure 1: SLAC data on the nucleon F_2^n/F_2^p ratio extracted from proton and deuteron DIS measurements [11] with a Fermi-smearing model [12].

Early SLAC experimental data in a limited x kinematical range ($0.1 \leq x \leq 0.3$) [13] reinforced an original naive view that the quark distributions functions $q_i(x)$ should not change in the nuclear medium, at least for small and medium values of x. Measurements by the European Muon Collaboration (EMC) [14] over a large-x range at CERN invalidated this view by observing a large x dependence for the ratio of the iron F_2^{Fe} per nucleon over

the deuteron F_2^d. This effect, the EMC effect, was confirmed in a subsequent analysis of old SLAC data [15], and an extensive study, using different nuclear targets, provided the exact x behavior of the effect versus the mass number A of nuclei [16]. The SLAC experimental data are shown in Figure 2 and indeed indicate a significant x and A dependence for the inelastic cross section ratio $(\sigma^A/\sigma^d)_{is}$ for several nuclei from ^{4}He to Au. The σ^A and deuteron σ^d cross sections are per nucleon and the ratio has been adjusted for an isoscalar nucleus of mass number A. This cross section ratio is equal to the equivalent isoscalar structure function ratio $(F_2^A/F_2^d)_{is}$.

2 Theory Overview

The F_2^n/F_2^p ratio can be calculated in a number of models of the nucleon. In a world of exact SU(6) symmetry, the wave function of a proton, polarized in the $+z$ direction for instance, would be simply [7]:

$$\begin{aligned} p\uparrow \;\; = \;\; & \frac{1}{\sqrt{2}} u\uparrow (ud)_{S=0} \;+\; \frac{1}{\sqrt{18}} u\uparrow (ud)_{S=1} \;-\; \frac{1}{3} u\downarrow (ud)_{S=1} \\ & -\frac{1}{3} d\uparrow (uu)_{S=1} \;-\; \frac{\sqrt{2}}{3} d\downarrow (uu)_{S=1} \;, \end{aligned} \tag{8}$$

where the subscript S denotes the total spin of the "diquark" partner of the quark. In this limit, the u and d quarks in the proton would be identical, and the nucleon and Δ isobar would, for example, be degenerate in mass. In deep-inelastic scattering, exact SU(6) symmetry would be manifested in equivalent shapes for the valence quark distributions of the proton, which would be related simply by $u_v(x) = 2d_v(x)$ for all x. For the neutron to proton F_2 structure function ratio this would imply [17]:

$$\frac{F_2^n}{F_2^p} \;=\; \frac{2}{3}, \qquad \frac{d}{u} = \frac{1}{2} \qquad \text{[SU(6) symmetry]}. \tag{9}$$

In nature, spin-flavor SU(6) symmetry is, of course, broken. The nucleon and Δ masses are split by some 300 MeV. In deep inelastic scattering off the nucleon, this symmetry breaking is reflected in the experimental observation that the d quark distribution is softer than the u quark distribution, with the F_2^n/F_2^p ratio deviating from the SU(6) expectation. The correlation between the mass splitting in the **56** baryons and the large-x behavior of

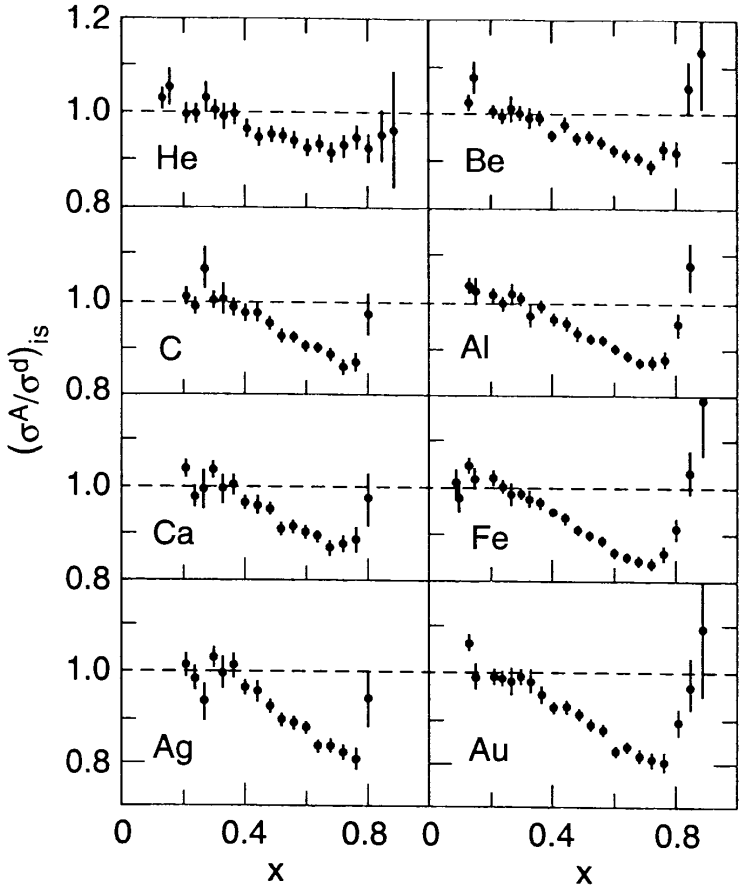

Figure 2: SLAC data on the inelastic cross section ratio of several nuclei (σ^A) to deuterium (σ^d) versus the Bjorken x [16]. The cross sections are per nucleon and the ratio has been adjusted for an isoscalar nucleus of mass number A.

F_2^n/F_2^p was observed some time ago by Close [18] and Carlitz [19]. Based on phenomenological [18] and Regge [19] arguments, the breaking of the symmetry in Equation 8 was argued to arise from a suppression of the "diquark" configurations having $S = 1$ relative to the $S = 0$ configuration as $x \to 1$. Such a suppression is in fact quite natural if one observes that whatever mechanism leads to the observed $N - \Delta$ splitting (e.g. color-magnetic force, instanton-induced interaction, pion exchange), it necessarily acts to produce a mass splitting between the two possible spin states of the two quarks which act as spectators to the hard

collision, $(qq)_S$, with the $S = 1$ state heavier than the $S = 0$ state by some 200 MeV [20]. From Equation 8, a dominant scalar valence diquark component of the proton suggests that in the $x \to 1$ limit, F_2^p is essentially given by a single quark distribution (i.e. the u), in which case:

$$\frac{F_2^n}{F_2^p} \;\to\; \frac{1}{4}, \qquad \frac{d}{u} \to 0 \qquad [S = 0 \text{ dominance}]. \tag{10}$$

This expectation has, in fact, been built into most phenomenological fits to the parton distribution data [21, 22, 23, 24].

The phenomenological suppression of the d quark distribution can be understood within the hyperfine-perturbed quark model of Isgur *et al.* [25, 26]. The color hyperfine interaction is generated by one-gluon exchange between quarks in the core. At lowest order, the Hamiltonian for the color-magnetic hyperfine interaction between two quarks is proportional to $\vec{S}_i \cdot \vec{S}_j$, where $\vec{S}_i$ is the spin vector of quark i. Because this force is repulsive if the spins of the quarks are parallel and attractive if they are antiparallel, from the SU(6) wave function in Equation 8 it naturally leads to an increase in the mass of the Δ and a lowering of the mass of the nucleon, and a softening of the d quark distribution relative to the u [26].

An alternative suggestion, based on a perturbative QCD argument, was originally formulated by Farrar and Jackson [27]. There it was shown that the exchange of longitudinal gluons, which are the only type permitted when the spins of the two quarks in $(qq)_S$ are aligned, would introduce a factor $(1 - x)^{1/2}$ into the Compton amplitude — in comparison with the exchange of a transverse gluon between quarks with spins anti-aligned. In this approach, the relevant component of the proton valence wave function at large x is that associated with states in which the total "diquark" spin projection, S_z, is zero as $x \to 1$. Consequently, scattering from a quark polarized in the opposite direction to the proton polarization is suppressed by a factor $(1 - x)$ relative to the helicity-aligned configuration.

A similar result is also obtained in the treatment of Brodsky *et al.* [28] (based on quark-counting rules), where the large-x behavior of the parton distribution for a quark polarized parallel ($\Delta S_z = 1$) or antiparallel ($\Delta S_z = 0$) to the proton helicity is given by: $q^{\uparrow\downarrow}(x) = (1 - x)^{2n-1+\Delta S_z}$, where n is the minimum number of non-interacting quarks (equal to 2 for

the valence quark distributions). Using Equation 8, in the $x \to 1$ limit one therefore predicts:

$$\frac{F_2^n}{F_2^p} \rightarrow \frac{3}{7}, \qquad \frac{d}{u} \rightarrow \frac{1}{5} \qquad [S_z = 0 \text{ dominance}]. \tag{11}$$

It should be noted that in the latter two treatments, the d/u ratio does not vanish as $x \to 1$ and the F_2^n/F_2^p ratio tends to 3/7 instead of 1/4.

Moving to the EMC effect, despite the intense theoretical work over the 20 years since its discovery, there is no unique theory or universally accepted model that describes its origin. There are many classes of models offering possible explanations of the effect. One class tries to explain the effect by revisiting the bound-nucleon problem and offering refined treatments for the nuclear binding and nucleon off-shellness. A second class attributes the existence of the effect to a possible increasing enhancement of the pion field, associated with the nucleon-nucleon interaction, with the nuclear mass number A. A third class departs from the conventional meson-nucleon framework of the nucleus and assumes that a dense nucleus with tightly packed nucleons has to be viewed and treated as a collection of multi-quark clusters. A distinct model in this class is one offering a quark-diquark structure of the nucleon, with the diquark modified in the nuclear medium. A fourth class is based on the idea of dynamical rescaling arising from the observation that iron F_2 structure function data resemble deuterium F_2 structure function data of higher Q^2 values. The underlying physical idea in this rescaling model is the change in the quark confinement scale of a nucleon embedded in a nucleus.

The above four classes are sometimes complemented by additional mechanisms that can offer explanations for the EMC effect pattern in specific x regions, like the well known shadowing mechanism, which reproduces the low-x pattern of the effect, and the increased Fermi momentum of the nucleons in heavier nuclei, which accounts for the large-x behavior of the EMC ratio data. The large number of approaches and models trying to explain the effect as well as comprehensive detailed accounts and comparisons of theoretical calculations with data are given in the excellent reviews of References [29, 30].

It is widely accepted that the first step in the understanding of the origin of the EMC effect is a realistic calculation of the structure function F_2 of the light, simplest nuclei in nature and in particular of the $A = 3$ mirror nuclei: ^{3}He and ^{3}H. Of paramount importance would

be a comparison of theory and experimental data for the ratio of the structure functions of the two nuclei, where both systematic and theoretical inherent uncertainties cancel out, making this ratio a benchmark for the understanding of the EMC effect [31].

3 Motivation for a New Experiment

Although the problem of extracting neutron structure functions from deuterium data is rather old [32], the discussion has been recently revived [33, 34, 35] with the realization [36] that F_2^n, extracted from F_2^p and F_2^d by taking into account Fermi-motion *and* binding effects in deuterium, could be significantly larger [34, 36] than that extracted in earlier analyses [12] in which only Fermi-motion corrections were applied.

Melnitchouk and Thomas [34] have incorporated binding and off-shell effects within a covariant framework in terms of relativistic deuteron wave functions (as calculated by Gross and collaborators [37], for instance). Neglecting the relativistic deuteron P-states and off-shell deformation of the bound nucleon structure function (which were found to contribute at the $\sim 1\%$ level [38]), the deuteron F_2^d structure function can be written as a convolution of the free proton and neutron F_2 structure functions and a nucleon momentum distribution in the deuteron, $f_{N/d}$:

$$F_2^d(x,Q^2) = \int dy\ f_{N/d}(y)\ [F_2^p(x/y,Q^2) + F_2^n(x/y,Q^2)], \tag{12}$$

where y is the fraction of the 'plus'-component of the nuclear momentum carried by the interacting nucleon, and $f_{N/d}(y)$ takes into account both Fermi-motion and binding effects. Their reanalysis of the SLAC data based upon this improved theoretical treatment led to larger F_2^n/F_2^p values as compared with the Fermi-motion only extracted values. As can be seen in Figure 3, the difference at $x = 0.85$ can be up to $\sim 50\%$.

Whitlow *et al.* [36] incorporated binding effects using the "nuclear density model" of Frankfurt and Strikman [39]. In this model, the EMC effect for the deuteron scales with nuclear density as for heavy nuclei:

$$\frac{F_2^d}{F_2^p + F_2^n} = 1 + \frac{\rho_d}{\rho_A - \rho_d}\left[\frac{F_2^A}{F_2^d} - 1\right]\ , \tag{13}$$

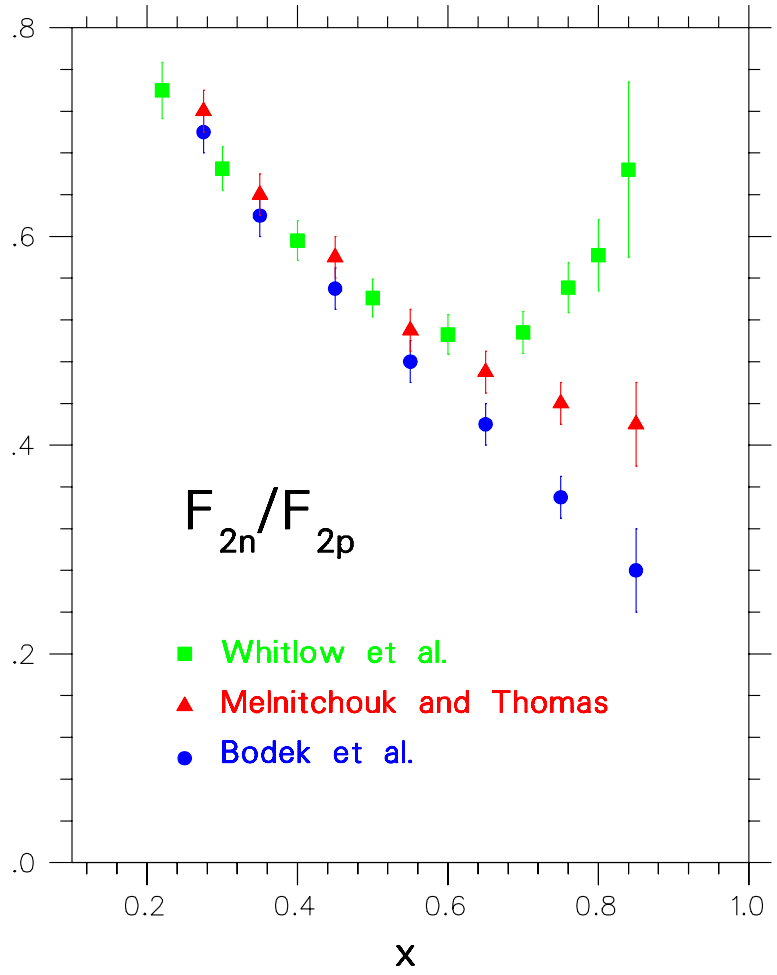

Figure 3: The F_2^n/F_2^p ratio extracted from proton and deuteron DIS measurements [11] with a) a Fermi-smearing model (Bodek *et al.* [12]), b) a covariant model that includes binding and off-shell effects (Melnitchouk and Thomas [34]), and c) the "nuclear density model" [39] that also incorporates binding and off-shell effects (Whitlow *et al.* [36]).

where ρ_d is the deuteron charge density, and ρ_A and F_2^A refer to a heavy nucleus with mass number A. This model predicts F_2^n/F_2^p values that are significantly higher ($> 100\%$) than the Fermi-motion only extracted ones at high x, as can be seen in Figure 3.

It is evident from the above two models that neglecting nuclear binding effects in the deuteron can introduce, at large x, a significant uncertainty in the extraction of the F_2^n/F_2^p and d/u ratios. A typical example for the magnitude of the uncertainty for the d/u ratio,

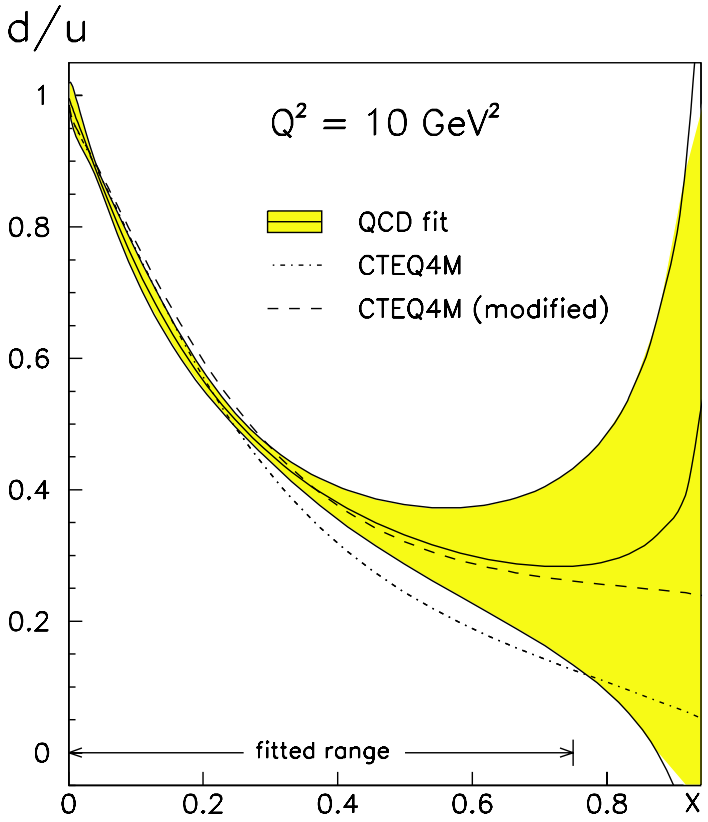

M. Botje, Eur. Phys. J. C14, 285-297, 2000

Figure 4: A typical uncertainty in the determination of the quark d/u distribution ratio by the QCD fit of Botje [40] on DIS cross section data. The solid curve is a QCD fit, and the shaded area shows the uncertainty in the fit. The dot-dashed curve represents the standard CTEQ4 fit [42], while the dashed curve corresponds to the CTEQ4 fit with a modified d quark distribution with $d/u \rightarrow \approx 0.2$ as $x \rightarrow 1$.

as estimated by one calculation from a QCD fit of proton and deuteron structure function data, is given in Figure 4 [40] (see also Ref. [41]). In the absence of experimental data or a unique theory for the magnitude of binding effects and the existence of the EMC effect in the deuteron, the question of the large-x behavior of F_2^n/F_2^p and d/u can only be settled by a measurement which does not rely on the use of the deuteron as an effective neutron target.

The above situation can be remedied by using a method proposed by Afnan *et al.* [43, 44], which maximally exploits the mirror symmetry of $A = 3$ nuclei and extracts the F_2^n/F_2^p ratio from DIS measurements off ^{3}H and ^{3}He. Regardless of the absolute values of the nuclear EMC effects in ^{3}He or ^{3}H, the differences between these will be small – on the scale of charge symmetry breaking in the nucleus – which allows for a determination of the F_2^n/F_2^p and d/u ratios at large-x values essentially free of nuclear contamination. At the same time, precise DIS measurements off ^{3}H and ^{3}He will provide the necessary structure function F_2 data for detailed studies of the EMC effect, which could lead to a canonical theory for the explanation of its dynamical origin. In summary, this method will, as it has been stated in Reference [31], i) unambiguously determine the valence u and d quark distributions of the free nucleon, ii) complete our knowledge of the EMC effect over the full range of nuclear mass number by determining the effect in the three-body systems and in the deuteron, and iii) provide valuable input in sorting out the change of the nucleon structure in the nuclear medium, which is fundamental to our understanding of QCD itself.

4 Exploring Deep Inelastic Scattering off ^{3}H and ^{3}He

In the absence of a Coulomb interaction and in an isospin symmetric world, the properties of a proton (neutron) bound in the ^{3}He nucleus would be identical to that of a neutron (proton) bound in the ^{3}H nucleus. If, in addition, the proton and neutron distributions in ^{3}He (and in ^{3}H) were identical, the neutron structure function could be extracted with no nuclear corrections, regardless of the size of the EMC effect in ^{3}He or ^{3}H separately.

In practice, ^{3}He and ^{3}H are of course not perfect mirror nuclei – their binding energies for instance differ by some 10% – and the proton and neutron distributions are not quite identical. However, the $A = 3$ system has been studied for many years, and modern realistic $A = 3$ wave functions are known to rather good accuracy. In a self-consistent framework one can use the same nucleon-nucleon (NN) interaction which describes the two-nucleon system to provide the basic input interaction into the three-nucleon calculation. Therefore, the wave functions can be tested against a large array of observables which put rather strong constraints on the models.

Defining the EMC-type ratios for the F_2 structure functions of ^{3}He and ^{3}H (weighted by corresponding isospin factors) by:

$$R(^3\mathrm{He}) = \frac{F_2^{^3\mathrm{He}}}{2F_2^p + F_2^n} \ , \qquad R(^3\mathrm{H}) = \frac{F_2^{^3\mathrm{H}}}{F_2^p + 2F_2^n} \ , \tag{14}$$

one can write the "super-ratio", $\mathcal{R}$, of these as:

$$\mathcal{R} \ = \ \frac{R(^3\mathrm{He})}{R(^3\mathrm{H})} \ . \tag{15}$$

Inverting this expression directly yields the ratio of the free neutron to proton structure functions:

$$\frac{F_2^n}{F_2^p} \ = \ \frac{2\mathcal{R} - F_2^{^3\mathrm{He}}/F_2^{^3\mathrm{H}}}{2F_2^{^3\mathrm{He}}/F_2^{^3\mathrm{H}} - \mathcal{R}} \ . \tag{16}$$

We stress that F_2^n/F_2^p extracted via Equation 16 does not depend on the size of the EMC effect in ^{3}He or ^{3}H, but rather on the *ratio* of the EMC effects in ^{3}He and ^{3}H. If the neutron and proton distributions in the $A = 3$ nuclei are not dramatically different, one might expect $\mathcal{R} \approx 1$. To test whether this is indeed the case requires an explicit calculation of the EMC effect in the $A = 3$ system.

The conventional approach employed in calculating nuclear structure functions in the valence quark region, $x > 0.3$, is the impulse approximation, in which the virtual photon, γ^*, mediating the electron-nucleus interaction, scatters incoherently from individual nucleons in the nucleus [29]. The nuclear cross section is determined by factorizing the γ^*–nucleus interaction into γ^*–nucleon and nucleon–nucleus amplitudes. The structure function of a nucleus, F_2^A, can then be calculated by folding the nucleon structure function, F_2^N, with the nucleon momentum distribution in the nucleus, $f_{N/A}$, as in Equation 12:

$$F_2^A(x) \ = \ \int dy \ f_{N/A}(y) \ F_2^N(x/y) \ \equiv \ f_{N/A}(x) \otimes F_2^N(x) \ , \tag{17}$$

where the Q^2 dependence in the structure functions is implicit. The convolution expression in Equation 17 is correct in the limit of large Q^2; at finite Q^2 there are additional contributions to F_2^A from the nucleon F_1^N structure functions, although these are suppressed by powers of M^2/Q^2. Corrections to the impulse approximation appear in the guise of final state interactions, multiple rescattering (nuclear shadowing), NN correlations and 6-quark

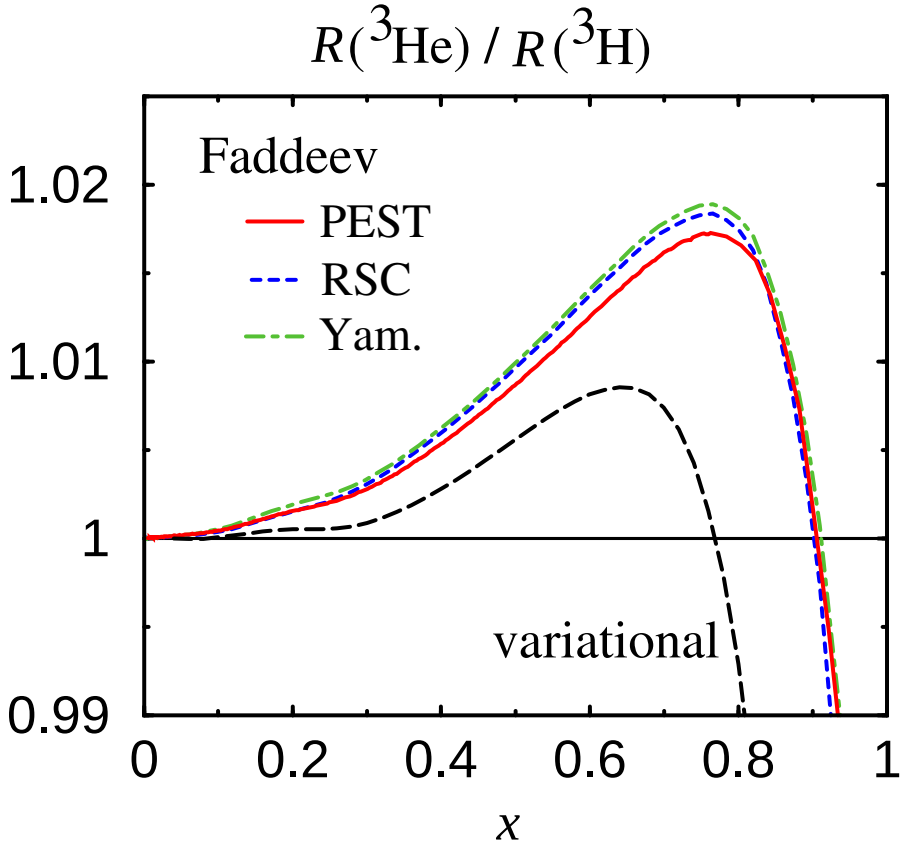

Figure 5: The "super-ratio" $\mathcal{R}$ of nuclear EMC ratios for ^{3}He and ^{3}H nuclei, with the nucleon momentum distribution calculated from the Faddeev (PEST, RSC, Yamaguchi) and variational (RSC) wave functions [44].

clusters, however, these are generally confined to either the small-x [45], or very large-x ($x > 0.9$) [46] regions.

The distribution $f(y)$ of nucleons in the nucleus is related to the nucleon spectral function $S(p)$ by [29]:

$$f(y) = \int d^3\vec{p} \left(1 + \frac{p_z}{p_0}\right) \delta\left(y - \frac{p_0 + p_z}{M}\right) S(p) \ , \tag{18}$$

where p is the momentum of the bound nucleon. For an $A = 3$ nucleus the spectral function is evaluated from the three-body nuclear wave function, calculated by either solving the homogeneous Faddeev equation with a given two-body interaction [43, 47] or by using a variational

technique [48]. The model dependence of the distribution function can be examined by using several different potentials. In Refs. [43, 44] a number of potentials were used, including the "EST" (Ernst-Shakin-Thaler) separable approximation to the Paris potential [49] [referred to as "Paris (EST)"], the unitary pole approximation [50] to the Reid Soft Core (RSC) potential, and the Yamaguchi potential [51] with 7% mixing between $^3S_1$ and $^3D_1$ waves. The Argonne AV18 potential [53] was also used for the calculations in Refs. [52, 54].

In terms of the proton and neutron momentum distributions, the F_2 structure function for ^{3}He is given by:

$$F_2^{^3\mathrm{He}} \;=\; 2\; f_{p/^3\mathrm{He}} \;\otimes\; F_2^p \;+\; f_{n/^3\mathrm{He}} \;\otimes\; F_2^n \;. \tag{19}$$

Similarly for ^{3}H, the structure function is evaluated from the proton and neutron momentum distributions in ^{3}H:

$$F_2^{^3\mathrm{H}} \;=\; f_{p/^3\mathrm{H}} \otimes\; F_2^p \;+\; 2\; f_{n/^3\mathrm{H}} \otimes\; F_2^n \;. \tag{20}$$

Because isospin symmetry breaking effects in nuclei are quite small, one can to a good approximation relate the proton and neutron distributions in ^{3}He to those in ^{3}H:

$$f_{n/^3\mathrm{H}} \approx f_{p/^3\mathrm{He}} \;, \qquad f_{p/^3\mathrm{H}} \approx f_{n/^3\mathrm{He}} \;, \tag{21}$$

although in practice both the isospin symmetric and isospin symmetry breaking cases have been considered explicitly. Note that even in the isospin symmetric case the proton and neutron distributions in ^{3}He will be different because while the neutron in ^{3}He is accompanied by a spectator pp, the spectator system of the proton is either an uncorrelated pn pair or a recoiling deuteron.

The ratio $\mathcal{R}$ of EMC ratios for ^{3}He and ^{3}H, as calculated by Afnan *et al.* [43, 44] is shown in Figure 5 for the various nuclear model wave functions [Paris (EST), RSC and Yamaguchi], using the CTEQ parametrization [24] of parton distributions at $Q^2 = 10$ (GeV/c)^2 for F_2^N. The EMC effects are seen to largely cancel over a large range of x, out to $x \sim 0.9$, with the deviation from unity of less than 2%. Furthermore, the dependence on the nuclear wave function is very weak. The pattern of behavior of the ratio $\mathcal{R}$ has been confirmed in independent calculations by Pace *et al.* [52], using a variational approach to calculate the

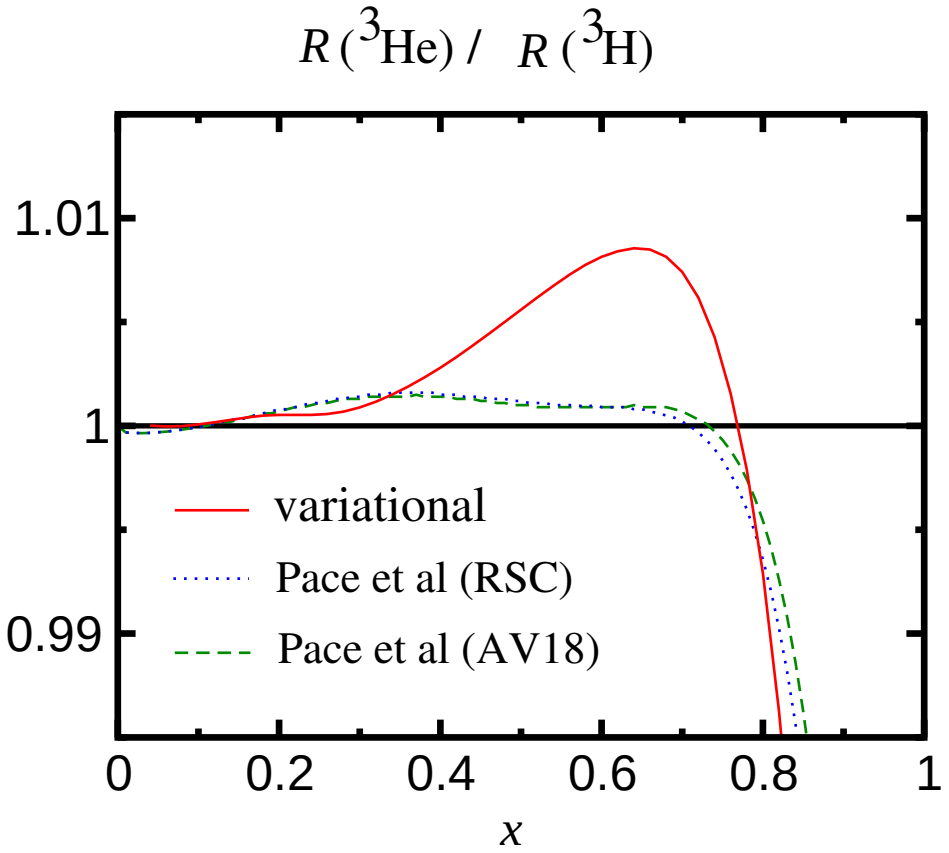

Figure 6: Ratio of nuclear EMC ratios for ^{3}He and ^{3}H for the variational calculation [44] (solid) and from Ref. [52] for the RSC (dotted) and AV18 (dashed) NN potentials (see text).

three-body spectral function, and by Sargsian *et al.* [54] using the Green function Monte Carlo wave functions from Ref. [53].

As seen in Figure 6, the deviation of $\mathcal{R}$ from unity is also well within the 2% range for both of the above cases. Note that the solid curve (from the work of Ciofi degli Atti and Liuti [55]) is computed using the RSC NN potential with the CTEQ parametrization of the nucleon structure function, while the dashed and dot-dashed curves (from Pace *et al.* [52]) use the RSC and AV18 potentials with the structure function fits from Ref. [56].

The dependence of $\mathcal{R}$ on the input nucleon structure function parametrization is illustrated in Figure 7, where several representative curves at $Q^2 = 10$ (GeV/c)^2 are given: apart from the standard CTEQ fit (solid), the results for the GRV [57] (dot-dashed), Donnachie-

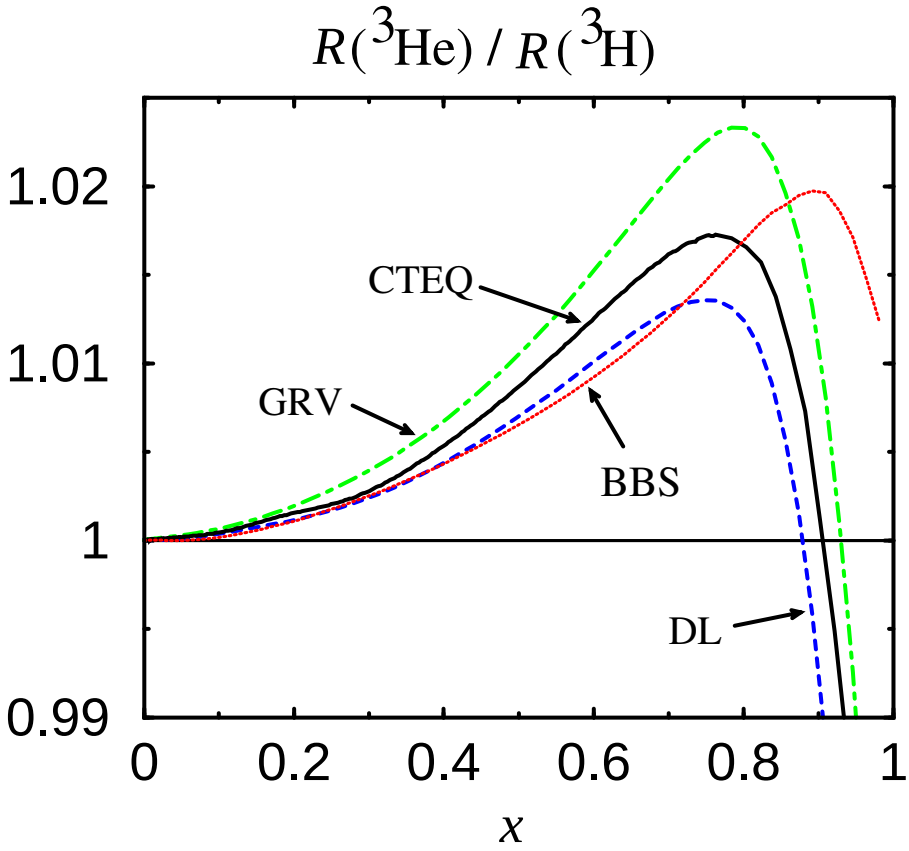

Figure 7: Ratio of nuclear EMC ratios for ^{3}He and ^{3}H with the Paris (EST) wave functions, using various nucleon structure function parametrizations [43] (see text): CTEQ (solid), GRV (dot-dashed), BBS (dotted), and DL (dashed).

Landshoff (DL) [58] (dashed), and BBS [28] (dotted) parametrizations are also shown (the latter at $Q^2 = 4$ (GeV/c)^2). For $x < 0.6$ there is little dependence ($< 0.5\%$) in the ratio on the structure function input. For $0.6 < x < 0.85$ the dependence is greater, but still with $< \pm 1\%$ deviation away from the central value $\mathcal{R} = 1.01$. The spread in this region is due mainly to the poor knowledge of the neutron structure function at large x. Beyond $x \approx 0.85$ there are few data in the deep-inelastic region on either the neutron or the proton structure functions, so here both the d and u quark distributions are poorly determined.

Despite the seemingly strong dependence on the nucleon structure function input at very large x, this dependence is actually artificial. In practice, once the ratio $F_2^{^3\mathrm{He}}/F_2^{^3\mathrm{H}}$ is

measured, one can employ an iterative procedure to eliminate this dependence altogether. Namely, after extracting F_2^n/F_2^p from the data using some calculated $\mathcal{R}$, the extracted F_2^n can then be used to compute a new $\mathcal{R}$, which is then used to extract a new and better value of F_2^n/F_2^p. This procedure is iterated until convergence is achieved and a self-consistent solution for the extracted F_2^n/F_2^p is obtained. Both Afnan *et al.* [43] and Pace *et al.* [52] have independently confirmed the convergence of this procedure.

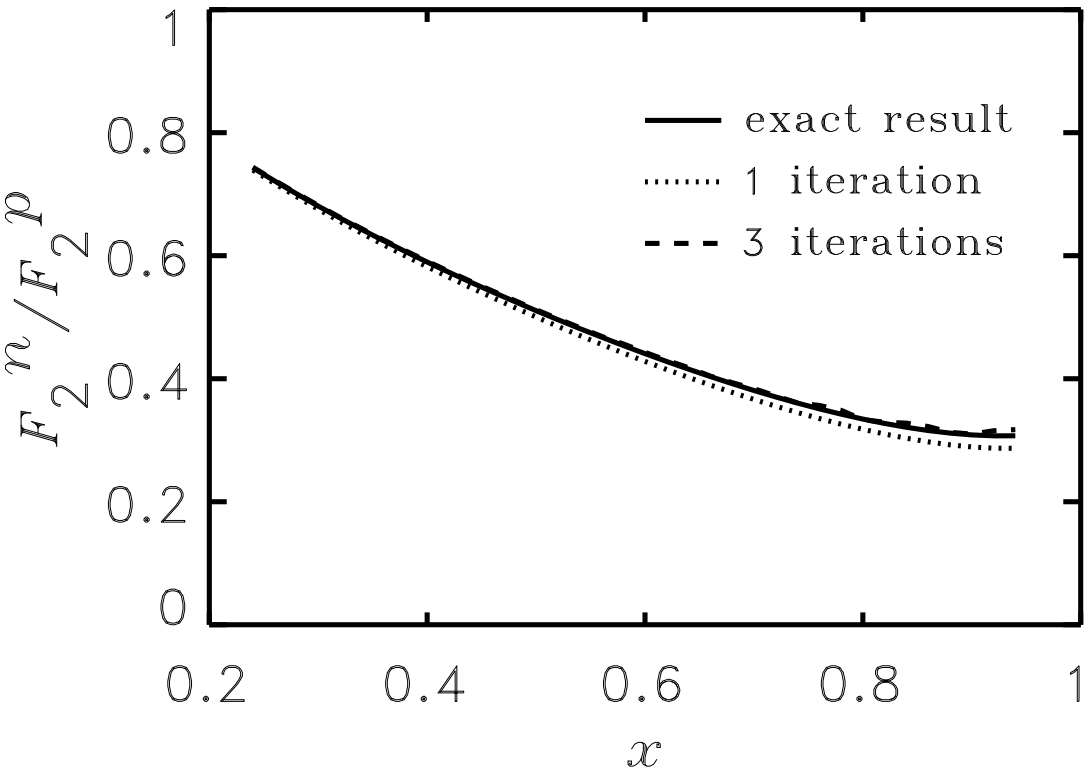

Figure 8: The convergence of the iterative procedure which eliminates the nucleon structure function dependence in the F_2^n/F_2^p extraction, from Ref. [44]. The input is $F_2^n/F_2^p = 1$, and the ratio after ~ 3 iterations is indistinguishable from the exact result (solid).

As an illustration, we show in Figure 8 the result from Afnan *et al.* [44] for different numbers of iterations using as input $F_2^n/F_2^p = 1$. The convergence is relatively rapid — by the third iteration the extracted function is almost indistinguishable from the exact result. Although the effect on $\mathcal{R}$ from the present lack of knowledge of the nucleon structure function

is $< 2\%$ for $x < 0.85$, this uncertainty can in principle be eliminated altogether via iteration, so that the only model dependence of $\mathcal{R}$ will be from the nuclear interaction in the $A = 3$ nucleus.

Of course the accuracy of the iteration procedure is only as good as the reliability of the above formalism and wave functions used to calculate the nuclear structure functions allows. The ratios in Figure 5 were calculated using three-nucleon wave functions neglecting the Coulomb interaction and working in an isospin basis (possible three-body forces can be omitted since these are expected to have a negligible effect on $\mathcal{R}$). To estimate the effect of neglecting the Coulomb interaction in ^{3}He and at the same time correct the long-range part of the three-body wave function due to the change in the binding energy, Afnan *et al.* [44] have modified the $^1S_0$ potential in ^{3}He and ^{3}H to reproduce their respective experimental energies. In this way the $^3S_1 - ^3D_1$ interaction responsible for the formation of the deuteron is unchanged. This approximation spreads the effect of the Coulomb interaction over both the *pp* and *np* interaction in the ^{1}S$_0$ channel, and to this extent, it shifts some of the Coulomb effects in the neutron distribution in ^{3}He to the proton distribution. However, this simple modification to the $^1S_0$ interaction allows one to study explicitly the possible effects associated with the differences in the binding energies of ^{3}He and ^{3}H.

The ratio $\mathcal{R}$ calculated in Ref. [44] with the Paris (EST) wave function modified according to this prescription is shown in Figure 9, labeled "Paris (EST)*" [the CTEQ parametrization of the nucleon structure function at $Q^2 = 10$ (GeV/c)^2 is used]. The result of this modification is a shift of $< 0.5\%$ in $\mathcal{R}$, with the net effect still being a ratio which deviates by $< 2\%$ from unity.

There are a number of other possible effects which could influence the ratio $\mathcal{R}$. Included in these is the Q^2 dependence of the structure functions, through higher order perturbative QCD corrections, higher twist terms, target mass corrections, and the choice of the form of the initial parton distributions. The impact of QCD corrections on the F_2^n/F_2^p ratio has been thoroughly investigated in Ref. [59]. Other uncertainties are inherent to the convolution formalism in a nucleus. The derivation of the convolution approximation in Equation 17 assumes that the nucleon off-shell dependence in the bound nucleon structure function is negligible. The off-shell dependence of F_2^N is, as a matter of principle, not measurable,

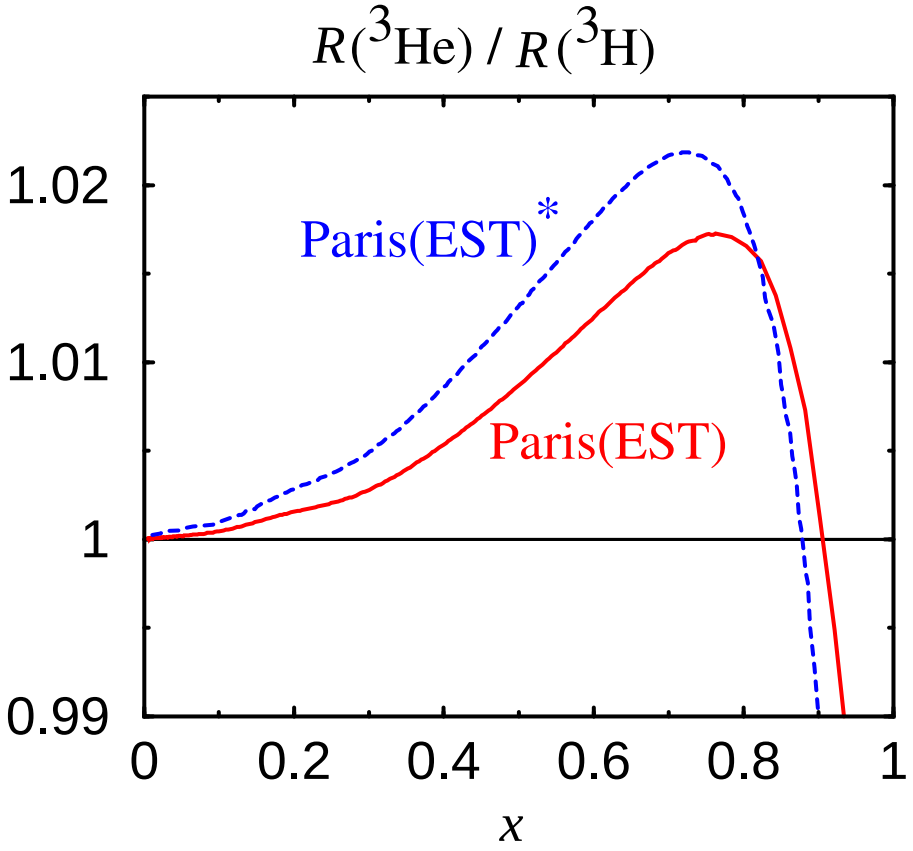

Figure 9: Ratio of nuclear EMC ratios for ^{3}He and ^{3}H for the Paris (EST) model (solid) and for the modified Paris (EST)* model (dashed) which includes explicit isospin symmetry breaking [43].

since one can always redefine the nuclear spectral function to absorb any p^2 dependence in the bound nucleon structure function. However, off-shell effects can be identified once a particular form of the interaction of a nucleon with the surrounding nuclear medium is specified. The discussion of off-shell modification of the nucleon structure function in the nuclear medium is therefore understood to be within the framework of the nuclear spectral functions defined in Equation 18.

Taking the nucleon's off-shellness into account, the bound nucleon structure function in Equation 17 can be generalized to [60, 61, 62]:

$$F_2^A(x,Q^2) \;=\; \int dy \int dp^2 \; \varphi(y,p^2,Q^2)\; F_2^N(x',p^2,Q^2)\;, \tag{22}$$

where $x' = x/y$ and the function $\varphi(y,p^2,Q^2)$ depends on the nuclear wave functions. In the absence of p^2 dependence in F_2^N, the light-cone momentum distribution $f(y,Q^2)$ in

Equation 17 would correspond to the p^2 integral of $\varphi(y, p^2, Q^2)$. In the approach of Ref. [60], the medium-modified nucleon structure function $F_2^N(x', p^2, Q^2)$ can be evaluated in terms of a relativistic quark spectral function which depends on the virtualities of the struck quark, k^2, and spectator system. The dependence of $k_{\rm min}$ on p^2 ($\neq M^2$) generates an off-shell correction which grows with A due to the A-dependence of the virtuality p^2 of the bound nucleon. This serves to enhance the EMC effect at large x in comparison with naive binding model calculations which do not take into account nucleon off-shell effects.

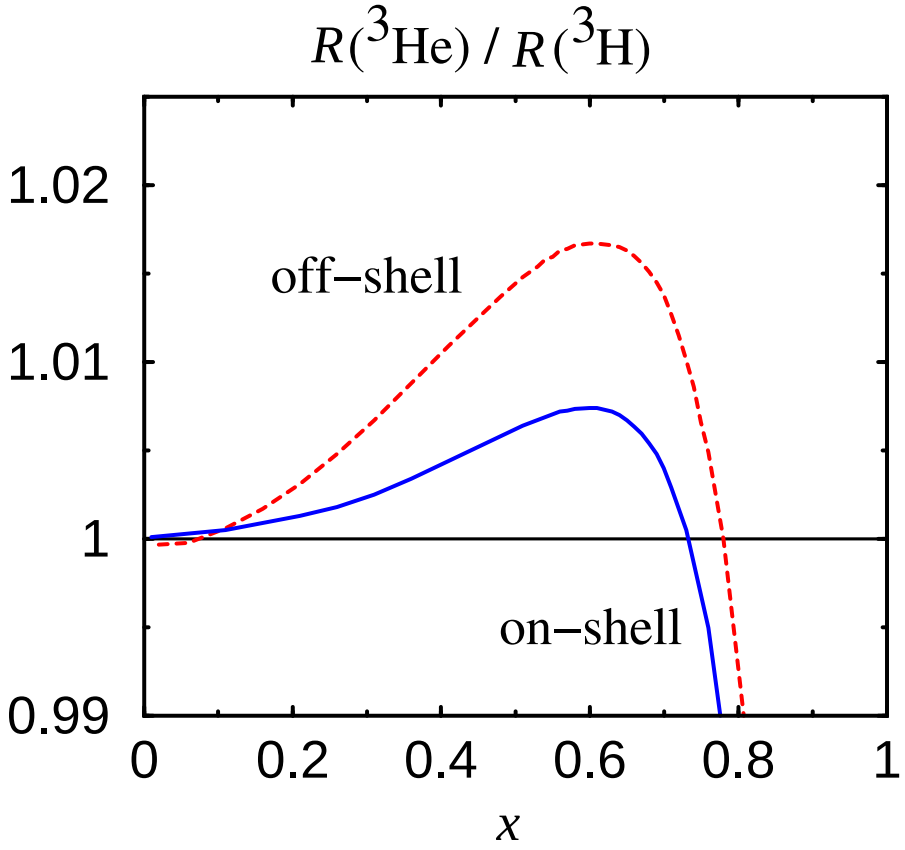

Figure 10: Ratio $\mathcal{R}$ of nuclear EMC ratios for ^{3}He and ^{3}H nuclei, with (dashed) and without (solid) nucleon off-shell corrections [60] (see text), for the variational (RSC) wave function.

The effect of the off-shell correction on the ratio $\mathcal{R}$, illustrated in Figure 10, is a small ($< 1\%$) increase in the ratio at $x \sim 0.6$. Off-shell effects of this magnitude can be expected in models of the EMC effect where the overall modification of the nuclear structure function arises from a combination of conventional nuclear physics phenomena associated with nuclear

binding, and a small medium dependence of the nucleon's intrinsic structure. Other models of the EMC effect, such as the color screening model for the suppression of point-like configurations (PLC) in bound nucleons [63], attribute most or all of the EMC effect to a medium modification of the internal structure of the bound nucleon, and consequently predict larger deviations of $\mathcal{R}$ from unity [54]. However, recent ^{4}He$(\vec{e}, e'\vec{p})$ polarization transfer experiments [64] indicate that the magnitude of the off-shell deformation is indeed rather small. The measured ratio of transverse to longitudinal polarization of the ejected protons in these experiments can be related to the medium modification of the electric to magnetic elastic form factor ratio. Using model independent relations derived from quark-hadron duality, the medium modifications in the form factors were related to a modification at large x of the deep inelastic structure function of the bound nucleon in Ref. [65]. In ^{4}He, for instance, the effect in the PLC suppression model was found [65] to be an order of magnitude larger than that allowed by the data [64], and with a different sign for $x > 0.65$. The results therefore place rather strong constraints on the size of the medium modification of the structure of the nucleon, suggesting little room for large off-shell corrections, and support a conventional nuclear physics description of the ^{3}He/^{3}H system as a reliable starting point for nuclear structure function calculations.

Corrections to the impulse approximation arising from the exchange of quarks between nucleons in $A = 3$ nuclei have been discussed by a number of authors [66, 67, 44, 54]. In Ref. [66] the effect on the EMC ratio, for the isospin-averaged $A = 3$ nucleus, was found to be comparable to that arising from binding. However, the analysis [66] did not allow for NN correlations, which are important at large momentum (and hence large x), so that the overall EMC effect is likely to have been overestimated. The effects of quarks which are not localized to single nucleons can alternatively be parametrized in terms of multi-quark clusters, in which six (or more) quarks form color singlets inside nuclei [68]. Six-quark configurations in the deuteron and other nuclei have been studied in a variety of observables, including nuclear electromagnetic form factors, NN scattering, as well as the EMC effect. Following Ref. [68], contributions from scattering off quarks in a six-quark cluster can be approximated by an effective six-quark structure function, $F_2^{6q}(x_{6q})$, in the nucleus, where $x_{6q} = Q^2/2M_{6q}\nu \approx x/2$. If P_{6q} is the probability of finding a six-quark cluster in the nucleus,

the net effect on the ^{3}He (and similarly ^{3}H) structure function can be approximated by:

$$F_2^{^3\mathrm{He}} \longrightarrow (1 - P_{6q}) F_2^{^3\mathrm{He}} + P_{6q} F_2^{6q} \ , \tag{23}$$

where $F_2^{^3\mathrm{He}}$ is the incoherent nucleon contribution.

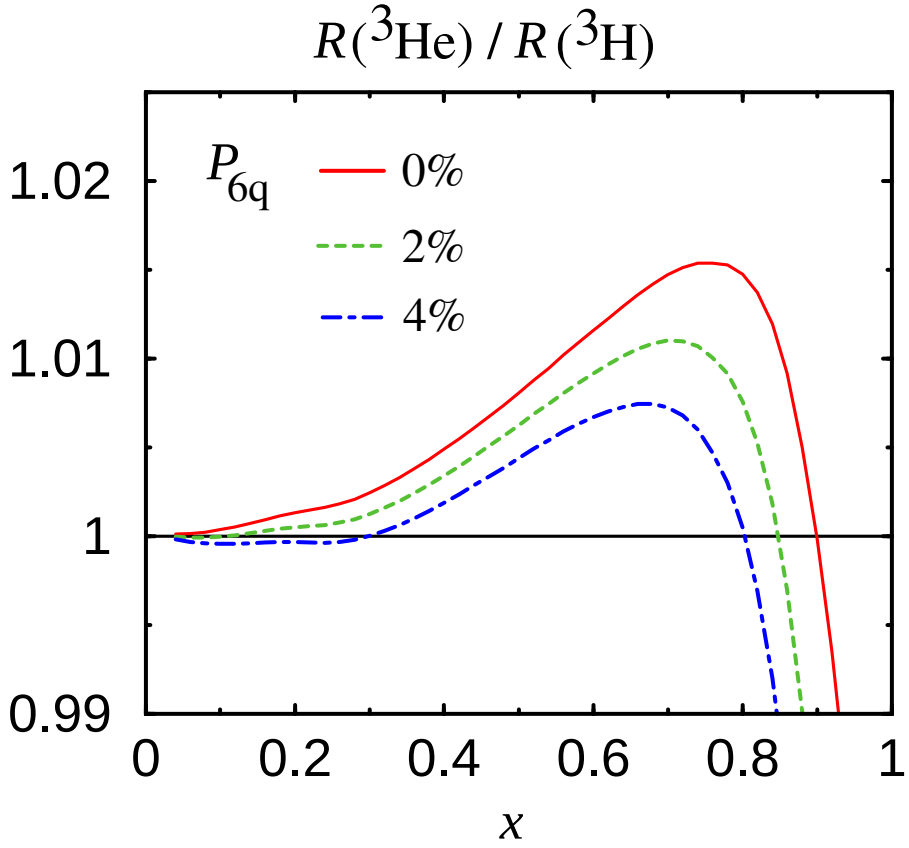

Figure 11: Ratio of nuclear EMC ratios for ^{3}He and ^{3}H for the Faddeev Paris(EST) wave function, with $P_{6q} = 0\%$, 2% and 4% six-quark configurations in the $A = 3$ wave function [44].

For a typical valence-like shape for F_2^{6q}, with the large-x behavior constrained by hadron helicity counting rules, $F_2^{6q} \sim (1 - x_{6q})^9$, Afnan *et al.* [44] have calculated the effect on $\mathcal{R}$ for $P_{6q} = 0\%$, 2% and 4%, shown in Figure 11. The overall effect is $< 1\%$ for all $x < 0.85$ even for the largest six-quark probability considered. For larger values of P_{6q} the deviation from unity is in fact even smaller, canceling some of the effects associated with nucleon off-shell dependence, for instance. Afnan *et al.* [44] and Sargsian *et al.* [54] have also considered

other six-quark structure functions, and while there is some sensitivity to the exact shape of F_2^{6q}, the $\sim 1\%$ effect on $\mathcal{R}$ appears to be an approximate upper limit for all x.

The analyses of the convolution model and the various extensions discussed in Refs. [43, 44, 52, 54] demonstrate the magnitude of the theoretical uncertainty in the calculation of the ratio $\mathcal{R}$. For the purpose of this proposal we assume that we can describe $\mathcal{R}$ with a central value and assign a systematic uncertainty that grows from 0.0% at $x = 0$ to $\pm 1.0\%$ at $x = 0.8$. Further theoretical investigations in the future could possibly reduce this uncertainty.

5 The Experiment

The upgraded 11 GeV beam of the Continuous Electron Beam Accelerator of Jefferson Lab offers a unique opportunity to perform deep inelastic electron scattering off the ^{3}He and ^{3}H mirror nuclei at large-x and Q^2 values. The DIS cross section for ^{3}H and ^{3}He is given in terms of their F_1 and F_2 structure functions by Equation 1, where M represents in this case the nuclear mass. The nuclear structure functions F_1 and F_2 are connected through the ratio $R = \sigma_L/\sigma_T$, where σ_L and σ_T are the virtual photoabsorption cross sections for longitudinally and transversely polarized photons, by:

$$F_1 = \frac{F_2(1 + Q^2/\nu^2)}{2x(1 + R)} \ . \tag{24}$$

The ratio R has been measured to be independent of the nuclear mass number A in precise SLAC and CERN measurements using hydrogen, deuterium, iron and other nuclei (for a compilation of data see References [29, 69]).

The direct substitution of Equation (24) into Equation (1) results in the elimination of F_1 in the inelastic cross section formula:

$$\sigma = \frac{4\alpha^2(E')^2}{Q^4} \cos^2(\frac{\theta}{2}) F_2 \left[\frac{1}{\nu} + \frac{(1 + Q^2/\nu^2)}{xM(1 + R)} \tan^2(\frac{\theta}{2})\right]. \tag{25}$$

By performing the tritium and helium measurements under identical conditions, using the same incident beam and scattered electron detection system configurations (same E, E' and θ), and assuming that the ratio R is the same for both nuclei, the ratio of the DIS cross sections for the two nuclei will provide a direct measurement of the ratio of their F_2 structure

functions:

$$\frac{\sigma(^3\mathrm{H})}{\sigma(^3\mathrm{He})} = \frac{F_2(^3\mathrm{H})}{F_2(^3\mathrm{He})}. \tag{26}$$

The key issue for this experiment will be the availability of a tritium target. Tritium targets have been used in the 1980's to measure the elastic form factors of ^{3}H at Saclay [70] and MIT-Bates [71]. The Saclay target contained liquid ^{3}H at 22 K and 20 atm. The tritium density was 0.260 g/cm^3 at the above operating conditions and was known to the $\pm 0.5\%$ level (based on actual density measurements). The activity of this target was 10 kCi. The MIT-Bates target [72] contained gas ^{3}H at 45 K and 15 atm. The tritium density was, under these operating conditions, 0.025 g/cm^3 with $\sim \pm 2\%$ uncertainty (based on a Virial formalism estimation), and its activity was 145 kCi.

Given a tritium target, an entire program of elastic [76], quasielastic [77] and inelastic [78] measurements will be possible at JLab [79]. Also measurements of semi-inclusive DIS $(e, e'\pi)$ reactions will be possible [80]. This entire program can, overall, be better accomplished in Hall A (which is envisioned also as the Hall for special setups in the 12 GeV era) by building a target similar to the MIT-Bates one. The target cell needed for this experiment is a 12 cm long stainless-steel cylinder with diameter of 1.5 cm, operating at the same conditions as the MIT-Bates target. The tritium density would be 0.025 g/cm^3, resulting in an activity of 5 kCi, which corresponds to the maximum amount of tritium handled commercially. This activity is about 30 times less than the Bates target activity. Two similar cells will also be necessary for the complementary ^{3}He measurements and for selected deuterium measurements. The deuterium measurements are highly desirable for checking the overall normalization of the cross section results and for diagnosing any scattered electron momentum and angle dependent effects. To eliminate background electrons scattering off the end-caps of the target cells, two adjustable, properly-machined tungsten collimating slits will be mounted on the support frame of the target system, right at the side of the cells. The slits will mask the spectrometer from the target end-caps, and at the same time they will define the effective target length seen by it.

The MIT-Bates target contained three subsystems: the tritium gas source, the target assembly, and the monitoring and controls systems [72]. The tritium gas source utilized a uranium-filled oven to safely store the tritium at room temperature as U^3H_2. Gas tritium

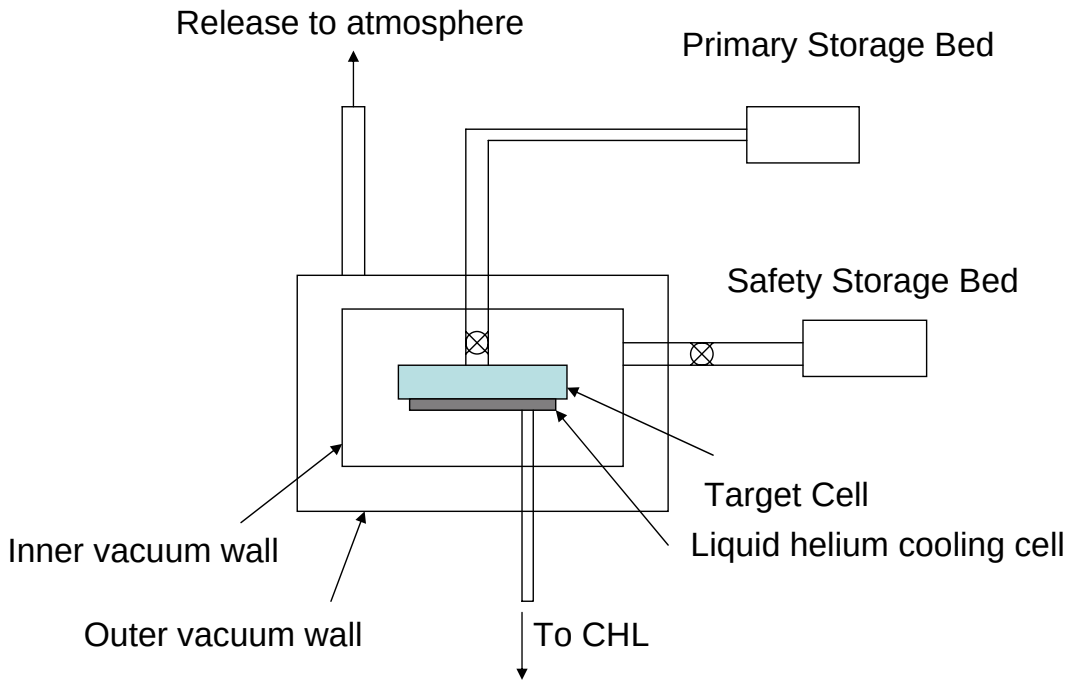

Figure 12: Schematic of the tritium target system (see text).

released from heating the uranium to about 440°C was transfered to a cool target cell (20 K), where it was liquified. After the tranfer was completed the oven was valved off and the target cell heated to the operating point of 45 K, thereby vaporizing the tritium. In emergency situations, the tritium could be quickly reabsorbed in the uranium by opening two parallel (for redundancy) valves. An empty spare oven was also included in the system as a backup to the primary oven.

A 40 W (20 K) helium refrigerator cooled the tritium MIT-Bates target cell. Temperature sensors were mounted in and on the cell, and target pressures were monitored on the transfer lines. Target temperature was controlled with heating coils placed on the target cell and refrigeration lines. The target assembly was surrounded by two concentric target enclosures, and was movable in the vertical direction to place various targets (including ^{3}He) in the beam path. The signals from numerous pressure and temperature sensors were received and processed by a microprocessor control system, which also monitored the state of binary devices (valves and heaters).

The safety requirements for the MIT-Bates target included 1) safe containment of the tritium inventory at all times with multiple layers of containment surrounding all tritium volumes, 2) quick and safe tritium storage in threatening or emergency situations, 3) fail-safe operation in case of power failure, 4) redundant procedural and equipment provisions for all operations and possible hazardous scenarios, 5) maximum dispersion of tritium in case of a containment breach, and 6) well trained operators chosen from the senior research staff of the laboratory [73, 74].

The principle of using a uranium beds to hold tritium is a well established method which is commercially available [75]. Uranium has a remarkable capacity for absorption of tritium. Once it has been properly prepared, one gram of uranium can hold about 360 Ci of tritium in the form of U^3H_3. The vapor pressure of $^3H_2$ over U^3H_3 slowly increases from 1.4×10^{-6} torr at room temperature, to 1 atm at 436° C. When the beds are at room temperature there is essentially no free tritium gas. By slowly increasing the temperature the tritium can be released in a controlled manner without risk of a sudden increase in pressure.

A very schematic view of the target system is shown in Figure 12. The bottom of the stainless-steel cell is covered by tubes filled with circulating liquid helium from the Central Helium Liquifier (CHL). The cell contains temperature and pressure gauges, and a resistive heater. By adjusting the flow of the helium and the power to the heater, the temperature of the cell can be adjusted to be cold enough to condense the tritium, or warm enough to return the tritium to a gaseous state.

The advantage of this system is the fact that no pumping is needed to return the tritium safely to its bed. The natural diffusion of the gas through the system quickly puts it into contact with the uranium, where it is completely captured in a few minutes.

The system has a number of safety features which make it a very low risk system. First, the valve between the beds and target is set to release in case of power failure or overpressure. The tritium will then be captured in the beds. Should the target fail, the tritium will be released into the first containment vessel. Whenever the target is in operation, the containment vessel will be connected to a second set of uranium storage beds. The volume of the containment is such that a complete release of the tritium will produce a pressure of only about one atmosphere. Surrounding the inner containment vessel will be an outer

containment vessel. This vessel can be exausted through a system leading to the top of the hall and into an exaust chimney which will eject the gas to the atmosphere. Even in this unlikely case, and assuming the tritium somehow is burned producing ^3H_2O (i.e. tritiated water), which is much more hazardous than $^3H_2$, the exposure to people at ground level will be below the accepted exposure level.

The actual target system will have many features not shown in the schematic in order to make an essentially fool-proof system, including shut off values to isolate the beam line in case of a leak, duplicate plumbing routes to allow both beds access to the system, pressure monitoring and tritium detectors at multiple locations.

The large solid angle of the Hall A High Resolution Spectrometers (HRS) will facilitate high-statistics DIS cross section measurements (less than one percent) in a large-x range as well as several valuable systematic checks. An important check would be to confirm that the ratio R is the same for ^{3}H and ^{3}He (it is known that R is the same for hydrogen, deuterium and several medium and heavy nuclei like Be, Fe etc). The performance of the above spectrometers is expected to be comparable, if not better, to that of the SLAC 8 GeV/c spectrometer that has provided precise measurements for absolute DIS cross sections, DIS cross section ratios, and differences in R for several nuclei [16, 81, 69]. The overall systematic errors for these measurements have been typically $\pm 2\%$, $\pm 1.0\%$ and ± 0.01, respectively. A similar JLab experiment using the HRS systems in Hall A will produce data of the same overall systematic uncertainties.

For the primary objective of the experiment, which is measurements of cross section ratios rather than absolute cross sections, many of the experimental errors that plague absolute measurements will cancel out. The experimental uncertainties on the ratio of cross sections should be similar to those achieved by SLAC experiments E139 [16] and E140 [81, 69], which were typically $\pm 1.0\%$ overall and $\pm 0.5\%$ point-to-point. It is a well known experimental fact that the best-determined cross sections and cross section ratios for inelastic electron scattering off nuclei have resulted from experiments using "small" solid angle traditional multi-element (quadrupoles and dipoles in tandem) magnetic systems like the SLAC 8 GeV/c spectrometer. The HRS systems are qualitatively similar to this SLAC spectrometer and will provide excellent cross section data with uncertainties comparable to the SLAC ones.

Inelastic scattering with the upgraded 11 GeV JLab electron beam can provide measurements of the ^{3}H and ^{3}He F_2 structure functions in the x range from 0.20 to 0.83. The electron scattering angle will range from 20° to 65° and the scattered electron energy from 1 to 3 GeV. The standard detector configuration of HRS with a Cherenkov counter and a lead-glass calorimeter, will provide discrimination between scattered electrons and an associated hadronic (mostly pion) background. The above two-counter combination has provided in the past a pion rejection factor of up to 10^5 to 1 [81] and has allowed DIS cross section measurements with negligible pion contamination up to a pion over electron ratio $\pi/e = 500$. The expected π/e ratio for this experiment has been estimated, using SLAC measurements of photon-nucleon cross sections [82], to be less than 300 at the highest-x kinematics. The pion contamination for a π/e ratio of 300 would be about 0.6%, which can be corrected with an estimated uncertainty of less than ±0.2%. The expected π/e ratio is given in Table 1 (Appendix I) along with the kinematical parameters for the proposed core set of measurements of the ratio $F_2(^3\mathrm{H})/\mathrm{F}_2(^3\mathrm{He})$ from $x \approx 0.20$ up to $x \approx 0.83$. The Table does not include the kinematics for the measurement of R or any other necessary systematic checks.

The estimated cross sections, counting rates and the beam times required for the above measurements are given in Table 2 (Appendix II). The core inelastic measurements for the structure functions of ^{3}He, ^{3}H and deuterium will be away from the nucleon resonance region with W^2 greater than 4.0 GeV^2. It will also be possible to measure the ^{3}He and ^{3}H structure functions at higher x values over the resonance region. [The quantity W is the invariant mass of the final hadronic state: $W = (M^2 + 2M\nu - Q^2)^{1/2}$.] Earlier studies of the proton F_2^p structure function in the nucleon resonance region [83] found that Bloom-Gilman duality (equivalence of the structure function averaged over the resonance region with the deep inelastic scaling function) worked to good accuracy for Q^2 down to $\sim$ 1 (GeV/c)^2. Phenomenological model studies [84] suggest that duality may work even better in the case of the neutron F_2^n structure function, so that for points with x greater than 0.83, the extracted F_2^n/F_2^p ratio could be interpreted in terms of the quark distribution ratio d/u. Furthermore, recent studies of ratios of nuclear cross sections at large values of x, between 0.6 and 0.8, strongly suggest that duality could be a good approximation for the highest Q^2 achievable at JLab [85]. This experiment will also be capable of checking the duality concept by measuring

the helium and tritium cross sections at several selected, large-x kinematics over the nucleon resonance region (for different values of W).

The expected scattered electron counting rates have been estimated, under the assumption that $\sigma(^3He) \simeq \sigma_d + \sigma_p$ and $\sigma(^3H) \simeq 2\sigma_d - \sigma_p$, using values for the proton (F_2^p) and deuteron (F_2^d) structure functions and for the ratio R from the "global" analysis of the SLAC DIS data [36]. The rates assume a 6 msr HRS solid angle and include, in an approximative way, radiative effects. It is evident from the listed rates that the proposed experiment will be able to provide very high-statistics data and perform necessary systematic studies in a very timely fashion. The required beam time for the x-scan of the helium and tritium cross sections, listed in Table 2, is 23 days for a canonical beam current of 70 μA. Inelastic scattering from the deuteron, at selected kinematics (not listed in the Table), will require two days of beam time. Also, a minimal study on the validity of duality for the helium and tritium inelastic data will require two days of beam time.

A very important systematic check will be to confirm, at selected kinematics, the expectation that the ratio R is the same for ^{3}H and ^{3}He. The 11 GeV beam and the momentum and angular range available by the HRS system can provide measurements of R in the same x range (0.2-0.7) as in the SLAC NPAS E140X experiment [69] by means of a Rosenbluth separation versus $\epsilon = [1 + 2(1 + \nu^2/Q^2)\tan^2(\theta/2)]^{-1}$ (the degree of the longitudinal polarization of the virtual photon mediating the scattering). Our R measurements will be limited by inherent systematics uncertainties rather than, as in the SLAC case, statistical uncertainties, and will be of the same or better precision as compared to the SLAC measurements. The large ϵ range $\Delta\epsilon > 0.50$ that can be achieved in this experiment will be a decisive factor for the accuracy of these measurements. The required beam time for the R measurements is three days for the canonical beam current of 70 μA.

The required precision of this experiment will necessitate very good knowledge of the spectrometer momentum acceptance. The most efficient and accurate method to accomplish this goal is to determine the spectrometer "acceptance function" by comparing deep inelastic deuterium cross section measurements from this experiment (taken with different central momentum configurations of the spectrometer) to a fit of the SLAC deuterium data, in con-

conjunction with a reliable optics/solid angle Monte Carlo model of the electron spectrometer. This method will require about one day of beam time.

6 Projected Experimental Results

The point-to-point uncertainties in the F_2^n/F_2^p determination will result from i) point-to-point uncertainties that do not cancel in the DIS cross section ratio of ^{3}H to ^{3}He ($\sim \pm 0.5\%$ as in SLAC experiment E140 [81]), ii) the theoretical uncertainty in the calculation of the super-ratio $\mathcal{R}$ (negligible at low x and growing up to $\sim \pm 1.0\%$ in the vicinity of $x = 0.8$), and iii) statistical uncertainties in the DIS cross section ratio of ^{3}H to ^{3}He (less than $\pm 1\%$). The overall normalization of the F_2^n/F_2^p ratio will be fixed by normalizing this experiment's low-x data for this ratio to the corresponding SLAC data, which at low x are free from theoretical uncertainties. The overall normalization error this way for the F_2^n/F_2^p ratio will be ± 0.01 [36].

The quality of the projected data on the F_2^n/F_2^p and d/u ratios, under the above conditions, is shown in Figures 13 and 14, respectively. The error bars include the point-to-point statistical, experimental systematic and theoretical uncertainties, and the overall normalization uncertainty, all added in quadrature. The shaded areas in Figures 13 and 14 indicate the present uncertainty, due mainly to possible nuclear corrections, in the extraction of F_2^n/F_2^p and d/u from hydrogen and deuterium inelastic data. It is evident that the proposed experiment will be able to unquestionably distinguish between the present competing extractions of the F_2^n/F_2^p and d/u ratios from proton and deuterium DIS measurements, and to determine their values with an unprecedented precision in an almost model-independent way.

It should be noted that a Jefferson Lab Hall B experiment has recently taken data to extract the neutron F_2^n structure function (BoNuS Experiment, E03-012) by measuring the cross section for semi-inclusive deep inelastic scattering off deuterium [86]. This experiment will provide F_2^n/F_2^p and d/u data from DIS scattering up to $x = 0.63$. The BoNus Collaboration plans to extend their measurements with the 11 GeV upgraded beam [87]. The x-range for DIS scattering ($W^2 > 4$ GeV^2) will be extended up to about $x = 0.77$, limited by the 40° maximum electron detection angle of the upgraded CLAS system.

BoNus has detected backward spectator protons in coincidence with the scattered electrons from the $e + d \rightarrow e + p_s + X$ inelastic reaction. The cross section for this process

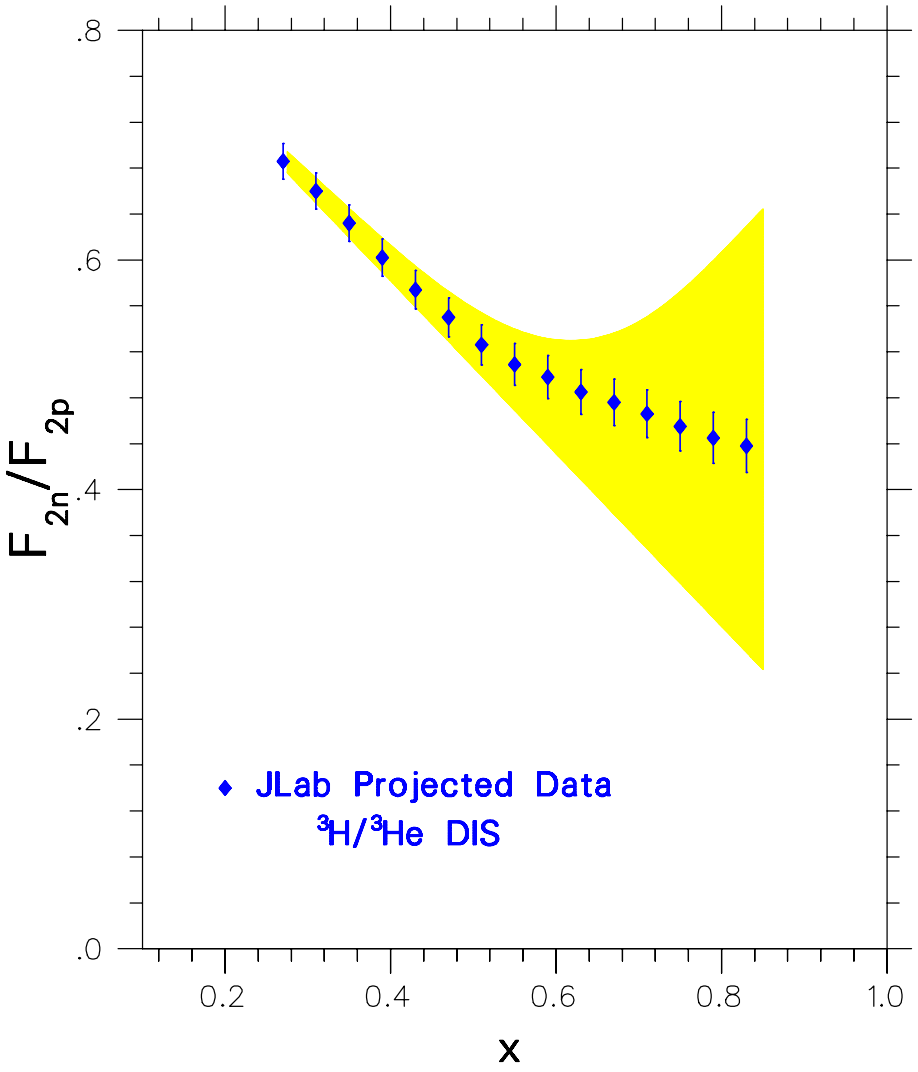

Figure 13: Projected DIS ($W^2 > 4$ GeV^2) data for the F_2^n/F_2^p structure function ratio from the proposed ^{3}H/^{3}He JLab experiment with a 11 GeV electron beam. The error bars include point-to-point statistical, experimental and theoretical uncertainties, and an overall normalization uncertainty added in quadrature. The shaded band indicates the present uncertainty due mainly to possible binding effects in deuteron.

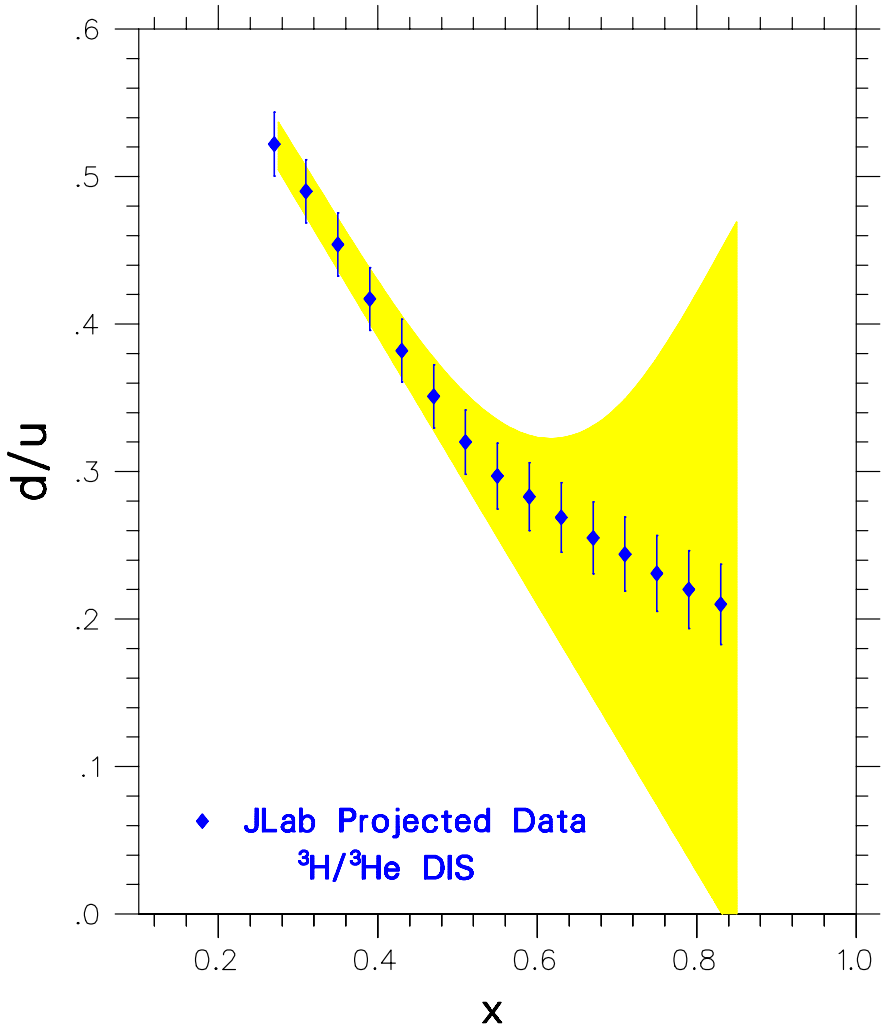

Figure 14: Projected DIS ($W^2 > 4$ GeV^2) data for the d/u quark distribution ratio from the proposed ^{3}H/^{3}He JLab experiment with a 11 GeV electron beam. The error bars include point-to-point statistical, experimental and theoretical uncertainties, and an overall normalization uncertainty added in quadrature. The shaded band indicates the present uncertainty due mainly to possible binding effects in deuteron.

is factorized in terms of the deuteron spectral function S and an effective neutron F_2 structure function:

$$\frac{d\sigma}{d^3p} \sim S(y,p^2)(F_2^n)_{eff}\left(\frac{x}{y},p^2,Q^2\right), \tag{27}$$

with:

$$y = \frac{M_d - E_s + (p_s)_z}{M_d}, \qquad p^2 = -\frac{p_t^2}{1-y} - \frac{y}{1-y}\left[M^2 - M_d^2(1-y)\right], \tag{28}$$

where p and p_s are the struck neutron and spectator proton four-momenta (with subscripts z and t denoting longitudinal and transverse components), E_s is the proton energy and M_d is the deuteron mass. This experimental approach is based on the isolation of the modifications in the structure of the bound nucleon within the impulse approximation, by choosing kinematics to minimize effects from the deuteron wave function and final-state interactions. It relies on the selection of backward low-energy proton kinematics to minimize: i) production of low-momentum protons from quark fragmentation, and ii) final-state interactions between the spectator proton and the neutron remnant. In addition, off-shell effects appear to be minimal for $p_s < 100$ MeV/c, which is expected to minimize uncertainties arising from the extrapolation of $(F_2^n)_{eff} \rightarrow (F_2^n)_{free}$. Extensive theoretical discussions of this method are given in Refs. [63, 88].

The expected statistical uncertainties on the F_2^n/F_2^p and d/u ratios are about the same for both ^{3}He/^{3}H and BoNuS E03-012 experiments, and overall smaller than the systematic uncertainties. Both experiments will normalize their data on the nucleon F_2 structure function ratio to the SLAC data at low x, which are free of theoretical uncertainties. The quality of data of the two experiments will be quantified by the point-to-point systematic uncertainties. The point-to-point total systematic error of the BoNuS experiment is, on the average, about twice as large as the projected point-to-point total systematic error of the ^{3}He/^{3}H DIS experiment. Although the quality of the projected results of the ^{3}He/^{3}H DIS experiment appears to be better than the BoNuS one, the two experiments are unequivocally highly complementary. Both results are expected to be pivotal for the determination of the nucleon F_2^n/F_2^p structure function and the d/u quark distribution ratios at large values of x.

The second goal of this $A = 3$ DIS experiment is the precise determination of the ratio of the EMC effect for ^{3}H and ^{3}He. At the present time, the available SLAC and CERN data allow for two equally compatible parametrizations [16] of the EMC effect, within the achieved experimental uncertainties. In the first parametrization, the EMC effect is parametrized versus the mass number A and in the second one versus the nuclear charge density ρ. While the two parametrizations are indistinguishable for heavy nuclei, they predict quite distinct

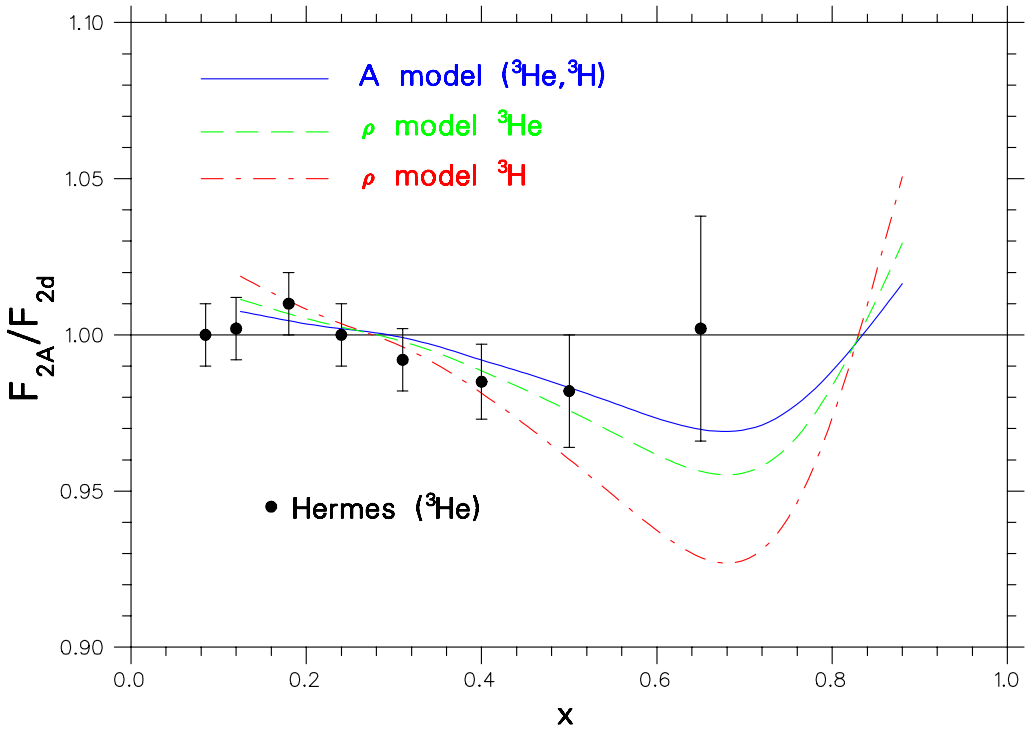

Figure 15: The ^{3}H and ^{3}He isoscalar EMC effect ratios $F_2(^3H)/F_2(d)$ and $F_2(^3He)/F_2(d)$ as predicted [16] by the nuclear mass A model (solid curve, ^{3}H and ^{3}He) and the nuclear density ρ model (dashed curve: ^{3}He, dot-dashed curve: ^{3}H). Also shown are recent data from the Hermes/DESY experiment [89].

patterns for $A = 3$. This is exhibited in Figure 15, which shows the isoscalar EMC effect ratios of ^{3}H and ^{3}He. The solid curve in Figure 15 assumes that the EMC effect scales with A and describes both $A = 3$ nuclei. The dashed and dot-dashed curves assume that the EMC effect scales with ρ, applied to ^{3}He and ^{3}H, respectively. Also shown in Figure 15 are available DESY-Hermes data [89] on the EMC effect for ^{3}He. (More data are expected in the near future from JLab Experiment E03-103 [90].)

The expected precision of this experiment for the $F_2(^3\mathrm{H})/F_2(^3\mathrm{He})$ ratio should easily allow for distinguishing between the two competing parametrizations and among theoretical calculations. This is demonstrated in Figure 16, which shows the ratio of the isoscalar DIS cross sections of the $A = 3$ nuclei for the two parametrizations and the associated

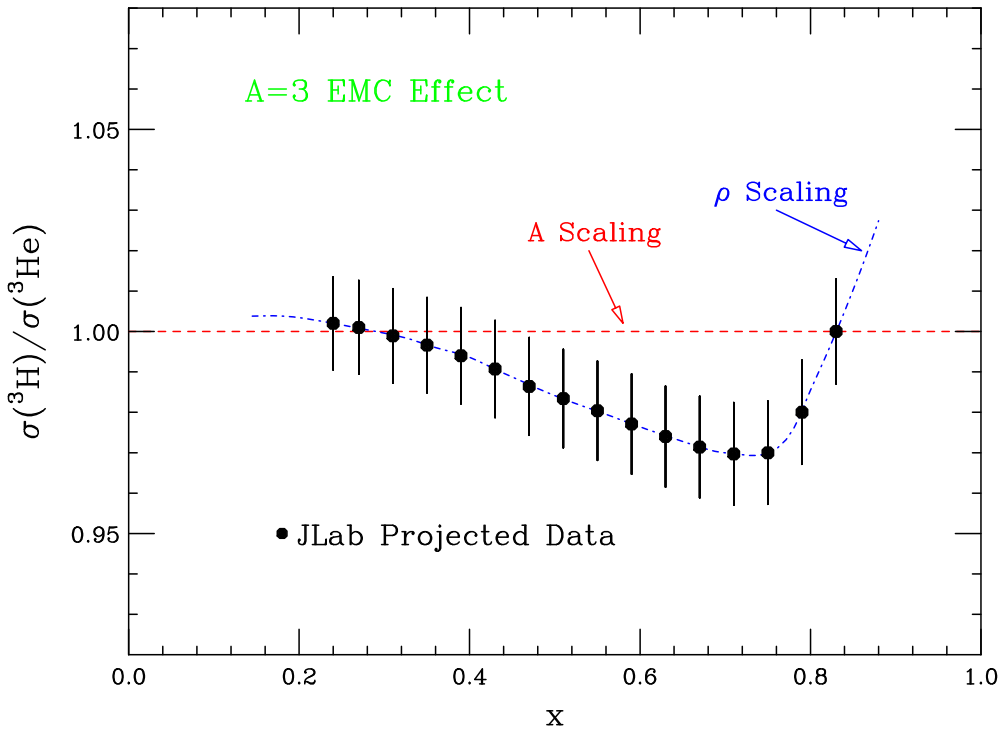

Figure 16: The ratio of the ^{3}H and ^{3}He isoscalar inelastic cross sections assuming that the EMC effect scales with the nuclear mass number A (dashed curve, i.e. the ratio is unity) or with nuclear charge density ρ (dot-dashed curve). Also shown are the projected data from this experiment, assuming arbitrarily that they follow the trend of the charge density parametrization of the EMC effect. The error bars include experimental systematic and statistical uncertainties added in quadrature.

projected data from this experiment, assuming that they arbitrarily follow the charge density parametrization. It should be noted that all available experimental data on the EMC effect determine the value of this ratio to be unity at $x = 0.3$. This will provide a power cross check of the normalization for the data of this experiment. The error bars in Figure 16 include experimental systematic and statistical uncertainties added in quadrature. It is evident that the proposed measurements should bring a closure to the EMC effect parametrization issue and provide crucial input for a complete, consistent explanation of the origin of the nuclear EMC effect.

Finally, it should be noted that several collaborating institutions have committed themselves to contribute to elements of the base instrumentation for the 12 GeV upgrade of Hall A, like the Arc energy measurement, which mainly involves designing and implementing the field mapping device of the ninth Arc dipole and performing the mapping (Kent State and St. Norbert), and the fast electronics upgrade for one of the two HRS systems (Rutgers).

7 Summary

We propose to perform deep inelastic electron scattering measurements off the $A = 3$ mirror nuclei using the 11 GeV upgraded beam of CEBAF and the Hall A Facility of Jefferson Lab. The experiment will require a cryogenic tritium/helium gas target system. The required beam time is one month (31 days) of beam time with a sufficient additional check-out time of the new gas target system. The measurements will determine in an almost model-independent way the fundamental F_2^n/F_2^p structure function and d/u quark distribution ratios at high Bjorken x, and distinguish between predictions based on perturbative QCD and non-perturbative models. The precision of these measurements will provide crucial input for the improvement of parton distribution parametrizations at high x, which are needed for the interpretation of high energy hadron collider data. The expected data will also test the validity of competing parametrizations and calculations of the nuclear EMC effect and provide crucial constraints on theoretical models for the explanation of its dynamical origin.

References

[1] R. E. Taylor, Rev. Mod. Phys. **63**, 573 (1991).

[2] H. W. Kendall, Rev. Mod. Phys. **63**, 597 (1991).

[3] J. I. Friedman, Rev. Mod. Phys. **63**, 615 (1991).

[4] E. D. Bloom *et al.*, Phys. Rev. Lett. **23**, 930 (1969); M. Breidenbach *et al.*, Phys. Rev. Lett. **23**, 935 (1969).

[5] J. I. Friedman and H. W. Kendall, Annu. Rev. Nucl. Sci. **22**, 203 (1972).

[6] J. D. Bjorken, Phys. Rev. **179**, 1547 (1969); J. D. Bjorken and E. A. Paschos, Phys. Rev. **185**, 1975 (1969).

[7] F. E. Close, *An Introduction to Quarks and Partons*, Academic Press, London (1979).

[8] F.J. Yndurain, *Quantum Chromodynamics*, Springer-Verlag, Berlin (1983); T. Muta, *Foundations of Quantum Chromodynamics*, World Scientific, Singapore (1987).

[9] R. P. Feynman, Phys. Rev. Lett. **23**, 1415 (1969).

[10] O. Nachtmann, Nucl. Phys. **B38**, 397 (1972).

[11] A. Bodek *et al.*, Phys. Rev. Lett. **30**, 1087 (1973); E. M. Riordan *et al.*, Phys. Rev. Lett. **33**, 561 (1974); J. S. Poucher *et al.*, Phys. Rev. Lett. **32**, 118 (1974).

[12] A. Bodek *et al.*, Phys. Rev. **D20**, 1471 (1979).

[13] S. Stein *et al.*, Phys. Rev. **D12**, 1884 (1975).

[14] J. J. Aubert *et al.*, Phys. Lett. **B123**, 275 (1983).

[15] A. Bodek *et al.*, Phys. Rev. Lett. **50**, 1431 (1983); Phys. Rev. Lett. **51**, 534 (1983).

[16] J. Gomez *et al.*, Phys. Rev. **D49**, 4348 (1994).

[17] J. Kuti and V. F. Weisskopf, Phys. Rev. **D4**, 3418 (1971).

[18] F. E. Close, Phys. Lett. **B43**, 422 (1973).

[19] R. Carlitz, Phys. Lett. **B58**, 345 (1975).

[20] F. E. Close and A. W. Thomas, Phys. Lett. **B212**, 227 (1988).

[21] E. Eichten, I. Hinchliffe, K. Lane and C. Quigg, Rev. Mod. Phys. **56**, 579 (1984).

[22] M. Diemoz *et al.*, Z. Phys. **C39**, 21 (1988).

[23] A. D. Martin, R. Roberts and W. J. Stirling, Phys. Rev. **D50**, 6734 (1994).

[24] H. L. Lai *et al.*, Phys. Rev. **D51**, 4763 (1995); H. L. Lai *et al.*, Eur. Phys. J. **C12**, 375 (2000).

[25] N. Isgur, G. Karl and R. Koniuk, Phys. Rev. Lett. **41**, 1269 (1978); N. Isgur, G. Karl and D. W. L. Sprung, Phys. Rev. **D23**, 163 (1981).

[26] N. Isgur, Phys. Rev. **D59**, 034013 (1999).

[27] G. R. Farrar and D. R. Jackson, Phys. Rev. Lett. **35**, 1416 (1975).

[28] S. J. Brodsky, M. Burkardt and I. Schmidt, Nucl. Phys. **B441**, 197 (1995).

[29] D. F. Geesaman, K. Saito and A. W. Thomas, Annu. Rev. Nucl. Part. Sci. **45**, 337 (1995).

[30] P. R. Norton, Rept. Prog. Phys. **66**, 1253 (2003).

[31] A. W. Thomas, hep-ex/0007029 (2000). In Proceedings of HiX2000 Conference, Philadelphia, Pennsylvania, April 2000.

[32] G. B. West, Phys. Lett. **B37**, 509 (1971); W. B. Atwood and G. B. West, Phys. Rev. **D7**, 773 (1973).

[33] S. Liuti and F. Gross, Phys. Lett. **B356**, 157 (1995).

[34] W. Melnitchouk and A. W. Thomas, Phys. Lett. **B377**, 11 (1996).

[35] U. K. Yang and A. Bodek, Phys. Rev. Lett. **82**, 2467 (1999).

[36] L. W. Whitlow *et al.*, Phys. Lett. **B282**, 475 (1992).

[37] W. W. Buck and F. Gross, Phys. Rev. **D20**, 2361 (1979); F. Gross, J. W. Van Orden and K. Holinde, Phys. Rev. **C45**, 2094 (1992); J. Adam, F. Gross, S. Jeschonnek, P. Ulmer and J. W. Van Orden, Phys. Rev. **C66**, 044003 (2002).

[38] W. Melnitchouk, A. W. Schreiber and A. W. Thomas, Phys. Lett. **B335**, 11 (1994).

[39] L. L. Frankfurt and M. I. Strikman, Phys. Rep. **160**, 235 (1988).

[40] M. Botje, Eur. Phys. J. **C14**, 285 (2000).

[41] S. I. Alekhin, Phys. Rev. **D63**, 094022 (2001).

[42] H. L. Lai *et al.*, Phys. Rev. **D55**, 1280 (1997).

[43] I. R. Afnan, F. Bissey, J. Gomez, A. T. Katramatou, W. Melnitchouk, G. G. Petratos and A. W. Thomas, Phys. Lett. **B493**, 36 (2000).

[44] I. R. Afnan, F. Bissey, J. Gomez, A. T. Katramatou, S. Liuti, W. Melnitchouk, G. G. Petratos and A. W. Thomas, Phys. Rev. **C68**, 035201 (2003).

[45] W. Melnitchouk and A. W. Thomas, Phys. Rev. **D47**, 3783 (1993) and Phys. Lett. **B317**, 437 (1993); G. Piller and W. Weise, Phys. Rep. **330**, 1 (2000).

[46] C. Ciofi degli Atti and S. Liuti, Phys. Lett. **B225**, 215 (1989); C. Ciofi degli Atti, S. Simula, L. L. Frankfurt and M. I. Strikman, Phys. Rev. **C44**, R7 (1991); S. Simula, Few Body Syst. Suppl. **9**, 466 (1995).

[47] F. Bissey, A. W. Thomas and I. R. Afnan, Phys. Rev. **C64**, 024004 (2001).

[48] C. Ciofi degli Atti, E. Pace and G. Salmè, Phys. Rev. **C21**, 805 (1980) and Phys. Lett. **B141**, 14 (1984).

[49] J. Haidenbauer and W. Plessas, Phys. Rev. **C30**, 1822 (1984).

[50] T. Y. Saito and I. R. Afnan, Few Body Syst. **18**, 101 (1995).

[51] Y. Yamaguchi, Phys. Rev. **95**, 1628 (1954).

[52] E. Pace, G. Salmè and S. Scopetta, Nucl. Phys. **A689**, 453 (2001); E. Pace, G. Salme, S. Scopetta and A. Kievsky, Phys. Rev. **C64**, 055203 (2001).

[53] S. C. Pieper and R.B. Wiringa, Ann. Rev. Nucl. Part. Sci. **51**, 53 (2001).

[54] M. M. Sargsian, S. Simula and M. I. Strikman, Phys. Rev. **C66**, 024001 (2002).

[55] C. Ciofi degli Atti and S. Liuti, Phys. Rev. **C41**, 1100 (1990) and Phys. Rev. **C44**, 1269 (1991).

[56] J. J. Aubert *et al.*, Nucl. Phys. **B293**, 740 (1987).

[57] M. Gluck, E. Reya and A. Vogt, Eur. Phys. J. **C5**, 461 (1998).

[58] A. Donnachie and P. V. Landshoff, Z. Phys. **C61**, 139 (1994).

[59] S. I. Alekhin, S. A. Kulagin and S. Liuti, Phys. Rev. **D69**, 114009 (2004).

[60] F. Gross and S. Liuti, Phys. Rev. **C45**, 1374 (1992).

[61] W. Melnitchouk, A. W. Schreiber and A. W. Thomas, Phys. Rev. **D49**, 1183 (1994).

[62] S. A. Kulagin, W. Melnitchouk, G. Piller and W. Weise, Phys. Rev. **C52**, 932 (1995); W. Melnitchouk, G. Piller and A. W. Thomas, Phys. Lett. **B346**, 165 (1995); G. Piller, W. Melnitchouk and A. W. Thomas, Phys. Rev. **C54**, 894 (1996).

[63] L. Frankfurt and M. Strikman, Nucl. Phys. **B250**, 143 (1985);

[64] S. Dieterich *et al.*, Phys. Lett. **B500**, 47 (2001); R. Ransome, Nucl. Phys. **A699**, 360 (2002).

[65] W. Melnitchouk, K. Tsushima, A. W. Thomas, Eur. Phys. J. **A14**, 105 (2002).

[66] P. Hoodbhoy and R.L. Jaffe, Phys. Rev. **D35**, 113 (1987).

[67] M. Betz, G. Krein and T.A.J. Maris, Nucl. Phys. **A437**, 509 (1985).

[68] P.J. Mulders and A.W. Thomas, Phys. Rev. Lett. **52**, 1199 (1984); M. Sato, S. Coon, H. Pirner and J. Vary, Phys. Rev. **C33**, 1062 (1986); K.E. Lassila and U.P. Sukhatme, Phys. Lett. **B209**, 343 (1988).

[69] L. H. Tao *et al.*, Z. Phys. **C70**, 387 (1996).

[70] A. Amroun *et al.*, Nucl. Phys. **A579**, 596 (1994); F.-P. Juster *et al.* Phys. Rev. Lett. **55**, 2261 (1985).

[71] D. H. Beck *et al.*, Phys. Rev. **C30**, 1403 (1984).

[72] D. H. Beck *et al.*, Nucl. Instr. Methods in Phys. Res. **A277**, 323 (1989).

[73] *The Tritium Gas Target System for the MIT-Bates Linear Accelerator Center, Final Safety Analysis Report*, MIT-Bates Laboratory (1985).

[74] *Tritium Target Standard Operating Procedures*, MIT-Bates Laboratory Report (1985).

[75] http://www.inus.com/docs/trisorb.htm

[76] J. R. Calarco, private communication.

[77] R. D. Ransome, private communication.

[78] G. G. Petratos *et al.*, nucl-ex/0010011 (2000), in Proceedings of HiX2000 Conference, Philadelphia, Pennsylvania, April 2000.

[79] R. D. Ransome, *A Tritium Program at 12 GeV*, presented at the Workshop on Physics of Nuclei with 12 GeV Electrons, Newport News, Virginia, November 2004.

[80] X. Jiang, private communication.

[81] S. Dasu *et al.*, Phys. Rev. **D49**, 5641 (1994).

[82] D. E. Wiser, Ph.D. Thesis, University of Wisconsin (1977).

[83] I. Niculescu *et al.*, Phys. Rev. Lett. **85** (2000) 1182, 1186.

[84] F. E. Close and N. Isgur, Phys. Lett. **B509**, 81 (2001); F. E. Close and W. Melnitchouk, Phys. Rev. **C68**, 035210 (2003).

[85] J. Arrington *el.*, Phys. Rev. **C73**, 035205 (2006).

[86] H. Fenker, C. Keppel, S. Kuhn, W. Melnitchouk *et al.*, JLab Proposal E03-012 (2003).

[87] *The Hall B 12 GeV Upgrade, Preconceptual Design Report*, Jefferson Lab (2004).

[88] S. Simula, Phys. Lett. **B387**, 245 (1996); W. Melnitchouk, M. Sargsian and M. Strikman, Z. Phys. **A359**, 99 (1997).

[89] K. Ackerstaff *et al.*, Phys. Lett. **B475**, 386 (2000).

[90] J. Arrington *et al.*, JLab Proposal E03-103 (2003).

APPENDIX I

Helium/Tritium DIS Kinematics for the F_2^n/F_2^p and d/u Extraction

x	W^2 (GeV)	Q^2 [(GeV/c)^2]	E (GeV)	E' (GeV)	θ (deg)	π/e
0.83	4.00	15.2	11.0	1.22	64.2	285
0.79	4.50	13.6	11.0	1.82	48.6	27
0.75	5.00	12.4	11.0	2.22	41.6	9
0.71	5.51	11.3	11.0	2.50	37.4	5
0.67	6.02	10.4	11.0	2.70	34.5	3
0.63	6.64	9.81	11.0	2.70	33.4	4
0.59	7.27	9.19	11.0	2.70	32.3	4
0.55	7.89	8.57	11.0	2.70	31.2	5
0.51	8.51	7.94	11.0	2.70	30.0	6
0.47	9.14	7.32	11.0	2.70	28.7	7
0.43	9.76	6.70	11.0	2.70	27.5	8
0.39	10.4	6.07	11.0	2.70	26.1	10
0.35	11.0	5.45	11.0	2.70	24.7	12
0.31	11.6	4.83	11.0	2.70	23.3	14
0.27	12.2	4.21	11.0	2.70	21.7	18
0.23	12.9	3.58	11.0	2.70	20.0	22

Table 1: The kinematics for the proposed ^{3}He and ^{3}H inelastic cross sections measurements for the extraction of the F_2^n/F_2^p and d/u ratios as a function of the Bjorken x. The beam energy, E, is fixed at 11.0 GeV. Here, W^2 is the squared invariant mass of the final hadronic state, Q^2 is minus the four-momentum transfer squared, E' is the scattered electron energy, θ is the scattered electron angle and π/e is the expected pion to electron counting ratio.

APPENDIX II

Cross Sections and Counting Rates for the F_2^n/F_2^p and d/u Extraction

x	$\sigma(^3\text{He})$ (nb/sr/GeV)	$\sigma(^3\text{H})$ (nb/sr/GeV)	^{3}He Rate (Events/h)	^{3}H Rate (Events/h)	^{3}He Time (h)	^{3}H Time (h)
0.83	0.0050	0.0042	107	188	234	133
0.79	0.0180	0.0142	524	884	57	34
0.75	0.0449	0.0348	1535	2535	23	14
0.71	0.0933	0.0715	3520	5770	11	6.9
0.67	0.174	0.133	7040	11600	6.4	3.9
0.63	0.266	0.205	11100	18300	4.0	2.5
0.59	0.398	0.310	17000	28400	2.9	1.8
0.55	0.583	0.461	25600	43300	2.1	1.3
0.51	0.842	0.675	38100	65200	1.7	1.0
0.47	1.20	0.978	55900	97100	1.5	1.0
0.43	1.70	1.41	81300	144000	1.0	1.0
0.39	2.40	2.02	118000	211000	1.0	1.0
0.35	3.38	2.89	170000	311000	1.0	1.0
0.31	4.80	4.18	247000	459000	1.0	1.0
0.27	6.89	6.11	362000	685000	1.0	1.0
0.23	10.1	9.14	538000	1040000	1.0	1.0

Table 2: Inelastic cross sections, counting rates and beam times for the different Bjorken x kinematics of the proposed ^{3}He and ^{3}H inelastic cross sections measurements for the extraction of the F_2^n/F_2^p and d/u ratios. The counting rates assume 12 cm, 45 K and 15 atm gas ^{3}He and ^{3}H targets, a beam current of 70 μA and a spectrometer solid angle of 6 msr.